

**Microfluidic Channels for Separation of Circulating Tumor Cells  
from Blood cells Using Dielectrophoresis and Performance  
Analysis Using ANFIS**

by

**Mir Ashib Ullah (170021128)  
Fazlul Rafeun Khorshed (170021142)  
Sadman Hoque (170021004)**

A Thesis Submitted to the Department of Electrical and Electronic Engineering in  
Partial Fulfillment of the Requirements for the Degree of

**BACHELOR OF SCIENCE IN ELECTRICAL AND ELECTRONIC  
ENGINEERING**



Department of Electrical and Electronic Engineering  
**Islamic University of Technology (IUT)**  
Gazipur, Bangladesh

May 2022

# **Microfluidic Channels for Separation of Circulating Tumor Cells from Blood cells Using Dielectrophoresis and Performance Analysis Using ANFIS**

Approved by:



-----  
**Dr. Md. Ruhul Amin**

Supervisor and Professor,  
Department of Electrical and Electronic Engineering,  
Islamic University of Technology (IUT),  
Boardbazar, Gazipur-1704.

Date: ..... 17/05/22

## **Declaration of Authorship**

This is to certify that the work in this thesis paper is the outcome of research carried out by the students under the supervision of Dr. Md. Ruhul Amin, Professor, Department of Electrical and Electronic Engineering (EEE), Islamic University of Technology (IUT).

### **Authors**



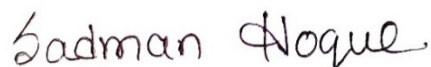
---

Mir Ashib Ullah  
ID- 170021128



---

Fazlul Rafeeun Khorshed  
ID- 170021142



---

Sadman Hoque  
ID- 170021004

## Table of Contents

<b>List of Tables .....</b>	<b>v</b>
<b>List of Figures.....</b>	<b>vi</b>
<b>List of Acronyms .....</b>	<b>viii</b>
<b>Acknowledgements.....</b>	<b>ix</b>
<b>Abstract.....</b>	<b>x</b>
<b>1 Introduction.....</b>	<b>1</b>
1.1 BACKGROUND.....	1
1.2 DIFFERENT WAYS TO MANIPULATE PARTICLES.....	1
1.3 PROBLEM STATEMENT .....	3
1.4 RESEARCH OBJECTIVES .....	4
1.5 RESEARCH MOTIVATION.....	5
<b>2 Literature Review .....</b>	<b>6</b>
<b>3 Dielectrophoresis and Fluid Dynamics .....</b>	<b>8</b>
3.1 INTRODUCTION .....	8
3.2 DEP ALONG WITH CLAUSIUS-MOSSOTTI FACTOR IN BRIEF .....	9
3.3 FLUID DYNAMICS .....	12
<b>4 Microfluidics in Lab-on-a-chip Technology.....</b>	<b>13</b>
4.1 LAB-ON-A-CHIP.....	13
4.1.1 <i>Innovation in Lab on a chip</i> .....	13
4.2 MICROFLUIDICS .....	14
4.2.1 <i>Applications</i> .....	15
4.3 MICROFLUIDIC DEVICES .....	15
4.3.1 <i>Material of Microfluidic Devices</i> .....	16
<b>5 Adaptive Neuro-Fuzzy Inference System (ANFIS) .....</b>	<b>17</b>
<b>6 Methods and Simulation Modelling.....</b>	<b>19</b>
6.1 METHODS .....	19
6.2 SIMULATION MODELING .....	21
6.3 MATERIAL AND PROPERTIES.....	22
6.4 MODELING AND GEOMETRY .....	23
<b>7 Results .....</b>	<b>26</b>
7.1 RESULTS FROM THE CHANNEL FOR SEPARATING CTCs FROM RBCS .....	26
7.1.1 <i>Mesh Analysis of the Channel</i> .....	26
7.1.2 <i>Results from Study 1</i> .....	27
7.1.3 <i>Results from Study 2</i> .....	28
7.1.4 <i>Results from Study 3</i> .....	29
7.1.5 <i>Effect of Shape and Design variation of the Microfluidic Channel on the Results of Study 3</i> .....	30
7.1.6 <i>Effect of Variation of Number of Electrodes of the Microfluidic Channel on the Results of Study 3</i> .....	31

7.1.7	<i>Effect of Variation of Electric Potential of Electrodes of the Microfluidic Channel on the Results of Study 3</i> .....	32
7.1.8	<i>Analysis of the Results from Simulation of the Microfluidic Channel using ANFIS</i> .....	35
7.1.9	<i>Separation Efficiency (SE) and Separation Purity (SP) of the Microfluidic Channel</i> .....	39
7.2	RESULTS OF THE CHANNEL FOR SEPARATING CTCs FROM WBCs AND RBCs .....	41
7.2.1	<i>Mesh Analysis of the Channel</i> .....	41
7.2.2	<i>Results from Study 1</i> .....	41
7.2.3	<i>Results from Study 2</i> .....	43
7.2.4	<i>Results from Study 3</i> .....	44
7.2.5	<i>Analysis of the Results from Simulation of the Microfluidic Channel using ANFIS</i> .....	45
7.2.6	<i>Separation Efficiency (SE) and Separation Purity (SP) of the Microfluidic Channel</i> .....	49
<b>8</b>	<b>Conclusion</b> .....	<b>51</b>
8.1	FUTURE WORKS.....	52

## List of Tables

<b>Table 6.1</b> Electrical and Flow Properties of Elements of the Simulation .....	23
<b>Table 6.2</b> Dimensions of the Microfluidic channel of Figure 3.2(a).....	25
<b>Table 6.3</b> Dimensions of the Microfluidic channel of Figure 3.2 (b) .....	25
<b>Table 7.1</b> Obtained Outputs with Respect to Inputs in COMSOL.....	35
<b>Table 7.2</b> Obtained Outputs with Respect to Inputs in COMSOL.....	46

## List of Figures

<b>Figure 3.1:</b> Response of the real part of the CM factor vs. Frequency for RBC, WBC and CTC.....	11
<b>Figure 5.1:</b> Five layers of ANFIS architecture with inputs x and y [28] .....	17
<b>Figure 6.1:</b> Flowchart of Simulation.....	19
<b>Figure 6.2:</b> Proposed microfluidic channels .....	20
<b>Figure 6.3:</b> Layouts of the proposed microfluidic channels with labeling for showing dimensions. ....	24
<b>Figure 7.1:</b> The two-dimensional meshed model of the dielectrophoretic separation channel which separates CTCs from RBCs .....	26
<b>Figure 7.2:</b> Spatial variation of (a) surface electric potential (V), (b) velocity ( $\mu\text{m/s}$ ), and (c) pressure (Pa).....	28
<b>Figure 7.3:</b> Particle Trajectories without application of any electric field .....	28
<b>Figure 7.4:</b> Particle Trajectories after application of non-uniform electric field (8V peak-to-peak).....	29
<b>Figure 7.5:</b> Particle trajectories for single phase separation model where separation failed at 8 V peak-to-peak applied voltage and $420\mu\text{m/s}$ inlet 1 fluid velocity and $260\mu\text{m/s}$ inlet 2 fluid velocity .....	30
<b>Figure 7.6:</b> Schematic and particle trajectories of the microfluidic channels having 8V peak-to-peak at the first region of separation electrodes failing to separate having (a) 3 electrodes in the first separation region and 3 electrodes in the second separation region; (b) 2 electrodes in the first separation region and 2 electrodes in the second separation region. ....	31
<b>Figure 7.7:</b> (a) Electric field distribution due to the applied voltages, simulation results of particle trajectories with $420\mu\text{m/s}$ inlet 1 fluid velocity and $260\mu\text{m/s}$ inlet 2 fluid velocity at (b) 6V peak-to-peak applied voltage at first phase electrodes and 4V peak-to-peak applied voltage at the second phase electrodes, (c) 8V peak-to-peak applied voltage at first phase electrodes and 4V peak-to-peak applied voltage at the second phase electrodes, (d) 10V peak-to-peak applied voltage at first phase electrodes and 4V peak-to-peak applied voltage at the second phase electrodes, and (e) 12V peak-to-peak applied voltage at first phase electrodes and 4V peak-to-peak applied voltage at the second phase electrodes. ....	34

<b>Figure 7.8:</b> (a) Neuro-Fuzzy Designer, and (b) ANFIS model structure .....	36
<b>Figure 7.9:</b> Effect of the fluid velocity at inlet 2 and electric potential of the electrodes on (a) outlet 3 fluid velocity ( $\mu\text{m/s}$ ), (b) maximum pressure (Pa) on the microfluidic channel, and (c) separation of CTCs and RBCs.....	38
<b>Figure 7.10:</b> Variation of (a) SE, and (b) SP of CTC with respect to applied peak-to-peak voltage on the first-phase electrodes (Keeping Inlet 1 velocity - $420\mu\text{m/s}$ , Inlet 2 velocity - $260\mu\text{m/s}$ , 2nd phase electrodes 4 V Peak-to-Peak as fixed quantities) .....	40
<b>Figure 7.11:</b> The two-dimensional meshed model of the dielectrophoretic separation channel which separates CTCs, RBCs and WBCs.....	41
<b>Figure 7.12:</b> Spatial variation of (a) surface electric potential (V), (b) velocity ( $\mu\text{m/s}$ ), and (c) pressure (Pa) .....	43
<b>Figure 7.13:</b> Particle Trajectories without application of any electric field .....	44
<b>Figure 7.14:</b> Particle Trajectories after application of non-uniform electric field (4V peak-to-peak).....	45
<b>Figure 7.15:</b> Effect of the buffer fluid velocity at inlet 2 and electric potential of the electrodes on (a) outlet 1 fluid velocity ( $\mu\text{m/s}$ ), (b) maximum pressure (Pa) on the microfluidic channel, and (c) separation of CTCs, RBCs and WBCs.....	48
<b>Figure 7.16:</b> Variation of (a) SE, and (b) SP of CTCs, RBCs and WBCs with respect to applied peak-to-peak voltage electrodes (Keeping Inlet 1 velocity - $150\mu\text{m/s}$ , Inlet 2 velocity - $700\mu\text{m/s}$ ) .....	50



## List of Acronyms

<b>AC</b>	Alternating Current
<b>ANN</b>	Artificial Neural Network
<b>ANFIS</b>	Adaptive Neuro-Fuzzy Inference System
<b>CM</b>	Clausius-Mossotti
<b>CTC</b>	Circulating Tumor Cell
<b>DC</b>	Direct Current
<b>DEP</b>	Dielectrophoresis
<b>DLD</b>	Deterministic Lateral Displacement
<b>EP</b>	Electrophoresis
<b>FEM</b>	Finite Element Method
<b>IDE</b>	Interdigitated Electrodes
<b>iDEP</b>	Insulator-based Dielectrophoresis
<b>LOC</b>	Lab-On-a-Chip
<b>MAP</b>	Magnetophoresis
<b>nDEP</b>	Negative Dielectrophoresis
<b>pDEP</b>	Positive Dielectrophoresis
<b>RBC</b>	Red Blood Cell
<b>RMSE</b>	Root Mean Square Error
<b>SE</b>	Separation Efficiency
<b>SP</b>	Separation Purity
<b>WBC</b>	White Blood Cell

## **Acknowledgements**

“In the name of ALLAH, Most Gracious, Most Merciful”

All the praises to Allah (SWT) for giving us the opportunity to complete this book. We would like to express our sincere gratitude to our supervisor, Dr. Md. Ruhul Amin. We are grateful for his patient guidance and valuable advice as without his help, diligence, insights, and enthusiasm, this work would never have been possible. We have gained a wealth of knowledge and experience through his direction that is beyond value to our future endeavors. We feel fortunate to have had the opportunity to work under his supervision. We are ever grateful to our parents for their lifelong encouragement, support, and attention and for being ravished patrons. We dedicate this work to them for their endless love, effort, and support. To our batch mates, seniors and friends, we thank them for everything they have done for us.

We would like to thank all the faculty members of the department of EEE, IUT for their inspiration and help. We also place record, our sense of gratitude to one and all, who directly or indirectly, have contributed to this venture.

## Abstract

The traditional isolation process of Circulating Tumor Cells (CTCs) is a huge technical hurdle. In this work, simple electrode arrangements are proposed that utilizes Dielectrophoresis and Fluid Dynamics to separate CTCs from blood cells that can be used effectively in microfluidic channels. Dielectrophoresis mechanism aided the microfluidic channel that has been made considering the Clausius-Mossotti (CM) factor, electrical and other mechanical properties of RBC and CTC particles to accumulate the rare CTCs being isolated from blood cells to a specified outlet. Single to multi-phase separation-based microfluidic channels have been proposed one of them can separate CTCs from RBCs in a comparatively low voltage of 8 V peak-to-peak in the first phase separation region and 4 V peak-to-peak in the second phase separation region with 100 kHz Alternating Current (AC) for the inlet sample stream speed of 420  $\mu\text{m/s}$ . The other microfluidic channel can separate CTCs from WBCs and RBCs in a comparatively low voltage of 6-8 V peak-to-peak with 100 kHz Alternating Current (AC) for the inlet sample stream speed of 150  $\mu\text{m/s}$ . A comparative analysis with microfluidic channels with single and multi-phase separation and different electrode arrangements by computer-assisted multi-physics simulations using Finite Element Method (FEM) with various governing parameters using COMSOL, MATLAB, and MyDEP software has been done in this study to validate the performance of the proposed microfluidic channels. The proposed microfluidic channels have achieved 100% separation efficiency (SE) and 100% separation purity (SP) while separating CTCs from different blood cells. Analysis of the inputs and outputs from the simulation models have been done to suggest specific values of inputs for the most efficient separation of the channels through Adaptive Neuro-Fuzzy Inference System (ANFIS) where two machine learning algorithms were used to give an overview of the microfluidic channel's input-output relationship.

# Chapter 1

## Introduction

### 1.1 Background

Microfluidics is a multidisciplinary area that involves physics, chemistry, engineering, and biotechnology, which has demonstrated efficacy in lab-on-a-chip (LOC) technologies lately [1]. The objective of the researchers working on LOC technology is to produce microfluidic chips that will enable healthcare professionals in poorly equipped clinics to conduct some diagnostic procedures with no laboratory assistance [2]. Based on the inertial properties of the cells, centrifugation technology processes samples for cell/microparticle separation. However, inertial characteristics of cells make it difficult to separate cells/particles with comparable inertial qualities [3]. Biological particle manipulation and separation using compact microfluidic devices is an emerging subject in clinical diagnostics. Since the introduction of the first microfluidic device in the 1970s, there has been an increase in attempts to build a broad range of microfluidic lab-on-a-chip (LOC) devices. These microfluidic devices have found applications in biotechnology, food processing, medical, mechanical, and chemical engineering, to mention a few [4]. Bioparticle separation has gained a lot of interest in LOC devices for biological and biomedical applications. Among the purposes of the newly introduced devices are the separation of healthy blood cells from sick ones, T-lymphocyte separation for HIV diagnosis, Circulating Tumor Cells (CTCs) separation for cancer detection.

### 1.2 Different ways to manipulate particles

Optical tweezers [5], magnetophoresis [6], acoustic means [7], and electrical means have all been developed for use in microsystems to manipulate particles.

**Optical tweezers:** In a method now known as optical tweezers, Ashkin and his colleagues at Bell Laboratories demonstrated that particles can be captured and manipulated employing highly focused laser beams [8] [9].

Refraction causes a light ray to leave any dielectric sphere at a different angle than it entered, implying that the light ray's momentum has changed. The sphere will experience an equal and

opposite momentum change, according to Newton's Third Law of Motion. We say that optical momentum has been transferred from the light beam to the sphere. When a spherical particle with a refractive index greater than the surrounding medium is shifted from the central axis of maximum light intensity, the stronger rays impart a larger momentum change towards the beam center than the weaker rays. This causes the sphere to be pushed to the maximum beam intensity. The laser beam will be pushed away from a spherical particle with a refractive index lower than that of the surrounding medium. [10]

**Magnetophoresis:** The polarization effect in a nonuniform magnetic field causes uncharged particles to move this phenomenon is known as Magnetophoresis (MAP) which shares a lot of the same interpretation and analysis as dielectrophoresis (DEP). The DEP-MAP analogy is limited in its utility because most magnetic particles are ferromagnetic and have high nonlinearity [11].

**Acoustic means:** An ultrasonic transducer mounted on the channel wall can apply an acoustic radiation force to a particle in a fluid stream. Piezoelectric ceramic rings are sandwiched and bolted between two metal blocks in this type of transducer. The piezoceramics expand when a DC voltage is applied to them, and the pressure applied to the blocks is transmitted into the bulk of the fluid. The frequency of an applied AC voltage causes the transducer to vibrate at that frequency, which is higher than that detectable by human ears.

There are two parts to the acoustic radiation force. The gradient of the wave's potential energy interacts with the compressibility difference between the particle and the fluid in one component, while the gradient of the kinetic energy interacts with the specific density differences between the particle and the fluid in the other. The particles are subjected to a force that is proportionate to their volume. As a result, large particles are subjected to a stronger acoustic force than small particles. [12]

Electrophoresis (EP) and dielectrophoresis (DEP) are subtle ways to control particles in LOC devices because EP and DEP have advantageous scaling for the smaller size of the system [13].

DEP has appeared to be a viable approach for a wide range of technical applications involving microparticles and nanoparticles manipulation [14]. DEP is the motion imparted on uncharged particles as a consequence of the polarization of them in the nonuniform electric fields [10]. There are several ways to manipulate particles in microsystems, but DEP is a popular choice

because of its label-free nature, scaling properties such that same force is achievable in a microscale system with lesser applied voltage than a macroscale system [13], ease of instrumentation, and ability to produce both attractive and repulsive forces. The DEP systems employ a low voltage alternating current (AC) rather than a high voltage direct current (DC) for the movement of particles, as in electrophoresis or electro-osmosis, and could be readily integrated with electronic detecting technologies like resistive and/or capacitive sensors to create an electronic LOC [15]. The DEP force is dependent on the particle size, the medium in which the particles are suspended, and electrical characteristics such as conductivity, permittivity, and frequency of the applied electric field. The particle does not have to be charged to use the DEP force. When an electric field is applied to systems containing particles suspended in a liquid, dipole moment is formed on the particles as a consequence of electrical polarizations at the particle-liquid interface [16].

### **1.3 Problem Statement**

There are two types of particle separation techniques:

- I. Passive separation
- II. Active separation.

Active separation methods depend on external force fields such as optical field [5], magnetic field [6], and acoustic field [7] to manage the targeted micro-particles within microchannel, while passive separation techniques depend solely on the structure of the microchannel and hydrodynamic forces [17]. As DEP shows higher sensitivity and precision operating at lower applied voltages [18], it has been utilized for manipulation of biological particles, such as cells [19], bacteria [20], viruses [21], yeast (*S. cerevisiae*) [21], and breast cancer cells [22].

In the initial stage, CTCs were detected in a patient's peripheral blood after blood was drawn from a patient's vein far from the original tumor. Those cells, according to the research, invaded and multiplied in other parts of the patient's body, producing secondary tumors inside the body

[23]. CTCs in the early phases of metastatic progression are crucial for studying malignant cells [24].

The most technical difficulty in CTC identification and separation is very low concentration of CTCs (1-3000 CTCs per mL) in comparison to the considerably higher amount of blood cells ( $10^9$  RBCs and  $10^6$  WBCs per mL) [25].

Single-cell purification is possible using DEP separation methods. But a low fluid velocity can make the procedure sluggish [26]. This indicates there is a trade-off between higher inlet velocity and the device structure which eventually leads to design single and multi-phase separation technique based microfluidic devices.

## **1.4 Research Objectives**

The sole purpose of this work is to develop microfluidic channels that can detect or isolate particles/ cells. Achieving this goal, the specific objectives have been considered as follows:

- Developing simpler designs for the microchannels.
- Simpler Electrode arrangement in the microchannels.
- Gaining higher efficacy utilizing less samples.
- Studying different effects of the microfluidic devices while changing different parameters.
- Developing label free detection technique which can be monitored in real time.
- Predicting different outputs from the microfluidic device for different inputs using ANFIS is another novelty of this work.

ANFIS incorporates human-like reasoning style through fuzzy logic systems while learns and computes using artificial neural networks (ANNs). ANFIS outperforms other modeling techniques such as ANNs, FIS, and multiple linear regression in most cases, according to the studies [27]. The term "adaptive" in ANFIS refers to the fact that some of the neurons in ANFIS

have changeable parameters that impact their outputs, and the learning rules determine the amount of change in these parameters to reach a minimum error [28].

## **1.5 Research Motivation**

Circulating tumor cells (CTCs) are a rare subset of cells found in blood of patients with solid tumors. The first stage to survive cancer is having hope to live. According to WHO (World Health Organization), 9.6 million worldwide are estimated to have died from cancer in 2018 due to different cancer variants. Biological particle separation and detection using compact microfluidic devices is a hot topic in biodefense and clinical diagnostics.

There has been a great boom in efforts to construct a wide variety of microfluidic lab-on-a-chip (LOC) devices since the advent of the first microfluidic device in the 1970s. However, LOC along with microfluidics is yet to be explored. This field has a lot more potential to help the community. As a result, researchers are currently working to maximize its use. The wish to give people a hope to fight against this disease is what motivated us to choose this topic as our thesis project.



## Chapter 2

### Literature Review

Kumar et al. developed an optimized microfluidic device to overcome the joule heating effect. The adjustment of the electric field at lower working voltages presents greater challenge in DEP, since higher voltages damage biological cells through joule heating, limiting the separation process. The device incorporated with tapered sidewall electrodes, provided an efficient separation of White Blood Cells (WBCs), RBCs and Platelets with higher electric field with lower excitation voltage. A maximum yield and purity are achieved with 1:5 velocity ratio for the two inlets of the device [3]. Krishna et al. modeled a microfluidic device with simple electrode arrangements avoiding interdigitated Electrodes (IDE) while utilizing two different voltages on the electrodes for separating microparticles based on size with sub-micron resolution. The performance is assessed in terms of separation efficiency and purity using the mathematical model. The residence period of the microparticles in the microchannel decreases as the volumetric flow rate increases, reducing the impact of nDEP forces on microparticles of both sizes, and therefore lowering the SP and SE [29]. Zhang et al. theoretically analyzed planar, semi-circular, and micro-pointed electrodes in different microfluidic device as experimental chips for separation of red blood cells and platelets. By comparing Electric field distribution of different shaped electrodes and the time needed to achieve the blood cell separation at the outlet, the microfluidic device is proposed for an optimal departure angle of 45 degree [30]. Alnaimat et al. presented a dielectrophoretic microfluidic flow separator which operates at a frequency of the applied electric field on the electrodes such that pDEP is experienced by the one type of particle, whereas nDEP is experienced by the other. With a large number of electrode pairs placed in larger spacing and a high applied electric voltage while maintaining a low flowrate, the device produces the desired output [31]. Aghaamoo et al. proposed a deterministic DEP design which combines the concept of deterministic lateral displacement (DLD) separation and iDEP techniques for uninterrupted separation of CTCs and WBCs, that has the potential for higher throughput and efficiency [32].

Ertugrul and Ulkir developed an optimized technique for a microfluidic device which separates platelets from red blood cells. For that two inlet and two outlets based microfluidic device

Ertugrul and Ulkir generated 16 rules with corresponding membership functions according to their problem to analyze the parameters of their modeled microfluidic device using fuzzy rules [33].

However, this work presents microfluidic devices consisting simpler electrode arrangements. These proposed devices utilize lower applied voltage while separating CTCs from RBCs and CTCs from WBCs and RBCs in microchannels with multi-phase to single phase separation region for attaining higher efficacy. These proposed microfluidic channels are analyzed through ANFIS. As, ANFIS offers broader selection of membership functions with powerful generalization capabilities, and superior explanation capabilities using fuzzy rules and ANN [34].

# Chapter 3

## Dielectrophoresis and Fluid Dynamics

### 3.1 Introduction

Dielectrophoresis (DEP) is the motion produced on a particle due to effect of an electric field which is not uniform in nature on an electrically neutral object. This phenomenon can be utilized to manipulate the motion of both organic and inorganic particles.

The consequence of a non-uniform electric field's presence on a particle ideal in nature (for example a perfect insulator) that can move freely, depends on the dielectric constant and the charge of the particle. If there is a net charge in the particle, it will result in an electrostatic interaction between the field and charge which causes motion in the particles. The resulting motion of the particles is called electrophoresis. If there exist permanent dipoles in the material, it will align with the field and extra force will be experienced by the particles towards the direction of the greatest electric field. That material will also have dipoles which are induced by the electric field and will normally be forced in the direction of increasing electric field strength. Such motion of neutral particles as a result of interaction of dipoles (either permanent or induced) with non-uniform electric field and expressed through dielectric constant is known as dielectrophoresis which was first termed by *Pohl* in 1951 [35]. The force created due to this motion is known as dielectrophoretic force. Dielectrophoresis has a much smaller effect as compared to electrophoresis.

If the particle is in any suspending fluid instead of being in a vacuum, in spite of that the fluid gets attracted by the electric field. The difference between the forces on each constituent separately is the resultant force on the particle. This force is proportional to the difference of their dielectric constants.

Muth in 1927 first studied the reaction of biological materials to electric fields. He noticed pearl-chain formation (attachment of particles as such that look similar to pearl chains) [36]. Schwan reviewed the electrical characteristics of tissue and cell suspensions in 1957. Pohl and Hawk (1966) were inspired by his observations of unusually high (effective) dielectric

constants ( $10^9$ - $10^4$ ) for cell and tissue suspensions to use selective dielectrophoresis to such a solution [37],38]. It was concluded that through the use of a perfect combination of solvent conductivity and frequency, the solely physical occurrence of dielectrophoresis could be used to distinguish between yeast cells which are dead and living yeast and also cause physical separation between the two types of cells. Crane and Pohl presented a more quantitative analysis of solution resistivity and frequency response in 1968 [39].

DEP is a process in which a non-uniform DC or AC electric field polarizes and moves suspended dielectric particles relative to the medium [40]. One distinctive characteristic of dielectrophoresis method is that DEP may be applied to both type of particles: charged and uncharged. Dielectrophoresis relies on the principle that a particle, for instance, when a biological cell is subjected to an applied electric field, that cell gets polarized electrically. Due to this an electric dipole moment ( $\vec{P}$ ) gets created. Equivalent and opposing charges ( $+Q$  and  $-Q$ ) will emerge on opposite ends of the particle, such that for a particle of diameter ( $\vec{d}$ ) the generated dipole moment is expressed as [10],

$$\vec{P} = Q\vec{d}, \quad (3.1)$$

the two opposite poles of the dipole moment do not feel similar electric force as there exists an electric field gradient. This causes the particles to deviate from its initial position. DEP is the reason for this deviation, and the force ( $\vec{F}_{DEP}$ ) that causes it is expressed as [10],

$$\vec{F}_{DEP} = (\vec{P} \cdot \nabla) \vec{E}, \quad (3.2)$$

where  $\vec{E}$  is the electric field imposed on a spherical dielectric particle, and  $\vec{P}$  is the dipole moment.

### 3.2 DEP along with Clausius-Mossotti Factor in Brief

The term Clausius-Mossotti factor is named after the Italian physicist Ottaviano-Fabrizio Mossotti. His book [41] written in 1850, analyzed the relationship between the dielectric constants of two different medium.

The complex Clausius-Mossotti (CM) factor involves the difference and sum of permittivity values. If the particle is spherical then the dielectrophoretic force acting on it is expressed as [25],

$$\overline{F_{DEP}} = 2\pi R^3 \varepsilon_m \varepsilon_0 \operatorname{Re}(f_{CM}) \nabla |\overline{E}|^2, \quad (3.3)$$

here  $R$  is the radius of the particle which is spherical in this case,  $\varepsilon_m$  represents surrounding medium's permittivity,  $\varepsilon_0$  represents permittivity of the vacuum,  $\nabla$  indicates the gradient operation and  $|\overline{E}|$  is the electric field's amplitude. The CM factor ( $f_{CM}$ ) is formulated as [10],

$$f_{CM} = \frac{\varepsilon_p^* - \varepsilon_m^*}{\varepsilon_p^* + 2\varepsilon_m^*}, \quad (3.4)$$

in (3.3) the real portion of CM factor is represented by  $\operatorname{Re}(f_{CM})$  defined as [10],

$$\operatorname{Re}(f_{CM}) = \frac{(\varepsilon_p - \varepsilon_m)(\varepsilon_p + 2\varepsilon_m) + \frac{\sigma_p - \sigma_m}{\sigma_p + 2\sigma_m} \omega}{(\varepsilon_p + 2\varepsilon_m)^2 + \left(\frac{\sigma_p + 2\sigma_m}{\omega}\right)^2}, \quad (3.5)$$

however,  $\varepsilon_p^*$  and  $\varepsilon_m^*$ , the complex permittivity of the particle and surrounding medium respectively in (3.4) are expressed as [25],

$$\varepsilon_p^* = \varepsilon_p \varepsilon_0 - j \frac{\sigma_p}{\omega}, \quad (3.6)$$

$$\varepsilon_m^* = \varepsilon_m \varepsilon_0 - j \frac{\sigma_m}{\omega}, \quad (3.7)$$

In (3.6) and (3.7),  $j = \sqrt{-1}$ ,  $\omega$  is the angular frequency ( $\omega = 2\pi f$ ) indicating the relationship between CM factor and the frequency ( $f$ ) of the applied electric field where the dependence of the complex parameters with the conductivity ( $\sigma_p, \sigma_m$ ) and permittivity ( $\varepsilon_p, \varepsilon_m$ ) of the surrounding medium and particle can be observed. Surrounded by a medium when a particle is subjected to an electric field, the charges inside both the particle and the surrounding media are redistributed. This charge results in the formation of an induced electric dipole causing opposite

charge distribution on each side of the particle. On application of a nonuniform electric field different forces will get created from each side of the particle [25].

It has been found that the real portion of the CM factor varies from -0.5 to 1 [42]. For the value ranging from 0 to 1, positive dielectrophoresis (pDEP) causes the particles to move where the electric field strength is high and for the value below zero of the real part of the CM factor, negative dielectrophoresis (nDEP) causes the particles to move where the the electric field strength is low.

The variation of the real part of the CM factor over a frequency ranging from  $10^3$  Hz to  $10^9$  Hz in the suspended fluid medium having conductivity of  $55\text{mS/m}$  has been evaluated in MyDEP software [43], shown below in **Figure 3.1**.

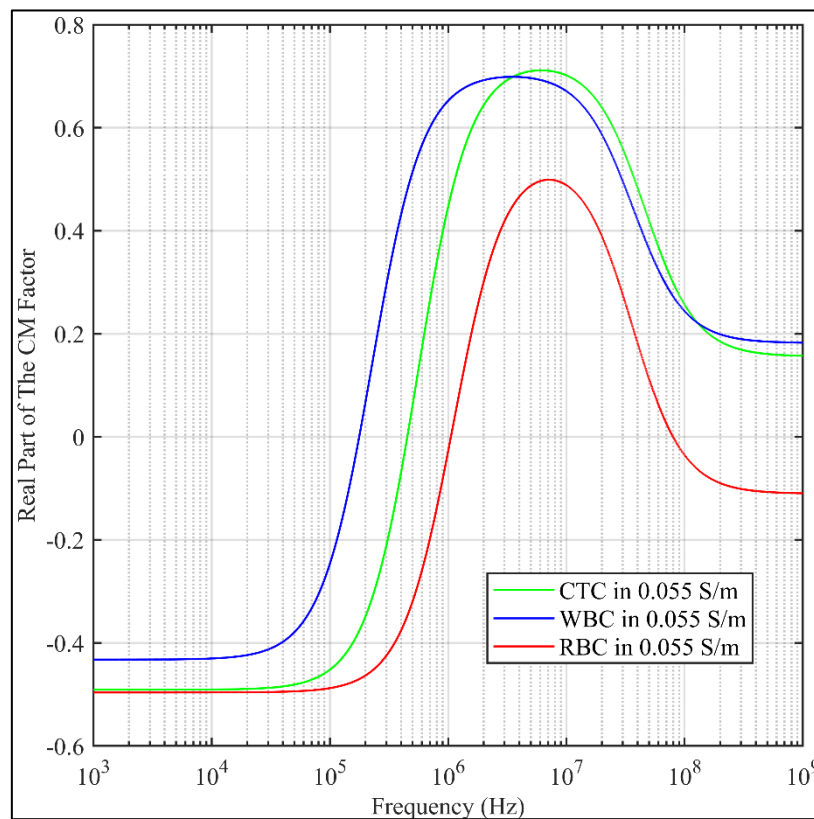


**Figure 3.1:** Response of the real part of the CM factor vs. Frequency for RBC, WBC and CTC

It has been observed from **Figure 3.1** that in low frequencies, the real part of the CTCs, WBCs and RBCs is negative which indicates the particles will experience nDEP. As a result, these particles will deviate to lower electric field region from higher electric field region. Because the DEP force is proportional to the cube of the particle radius, particles having a larger radius

are exposed to a greater DEP force than those with a smaller radius. Also, the DEP force is proportional to the square of the electric field gradient [44].

### 3.3 Fluid Dynamics

Fluid dynamics serves an important role in particle movement, particularly in microfluidics, as surface forces are prominent in regulating various fluid properties like flow velocity, turbulence, and so on. A crucial parameter Reynolds number [45] expressed as,

$$Re = \frac{\rho V D}{\mu}, \quad (3.8)$$

Reynolds number being a function of the fluid density ( $\rho$ ), velocity ( $V$ ), diameter ( $D$ ), dynamic viscosity ( $\mu$ ) used in (3.8) is used to characterize the fluid flow in a microchannel. The Reynolds number is a dimensionless parameter which is important for describing flow circumstances. It is a combination of fluid qualities, geometric properties, and the typical flow speed, and it is not merely a property of the fluid.

Due to laminar flow molecular transportation towards the outlets is generally foreseeable. As the fluid which has been used for this work has a high viscosity and flows through a microchannel at low speed, the Reynolds number is less than one ( $Re < 1$ ). High value of Reynolds number introduces complexity in flow tending towards turbulence flow. Because low Reynolds number flows are generally laminar, the two fluids can flow side by side down the channel in the absence of major density changes, allowing the streams to be controlled and manipulated.

It is essential to understand that the velocity of the flow used to move the suspended cells/particles in the microchannel varies across the channel. Cells/particles move at the fastest at or near the middle of the channel and at the slowest (zero) towards the edges. There is a natural dispersion of suspended materials because different points in the fluid flow at different speeds. This enables fine control at short length scales, making fluid dynamics an important component in the approach for developing Lab-on-a-chip devices using dielectrophoresis.

# Chapter 4

## Microfluidics in Lab-on-a-chip Technology

### 4.1 Lab-on-a-chip

Micro complete analyzing systems, also known as lab-on-a-chip systems, are unified microelectromechanical mechanisms that can perform all phases of biochemical processes. They allow for the downsizing and integration of complicated functionalities, allowing for the automation of routine laboratory procedures. Lab-on-a-chip devices' mobility, easy to carry, and parallelization benefits point-of-care diagnostics. A full lab-on-a-chip must be capable to perform common laboratory activities like crude sample handling, sample and reagent mixing and reacting separation and analytic detection. Particular conventional functional elements, each with a various role to play, can be assembled on an individual chip to achieve the mentioned functions that deal with sample analysis and processing. [46]

Lab-on-a-chip has long been thought to be one of, if not the most concise, methodologies for incorporating research lab biochemical methodologies into nano-sized, reduced introspective devices for mobile screening procedures in a variety of collection scenarios, aided by the use of microfluidic systems and biosensing. This technology has progressed to the point that a variety of inventive devices and components may now perform a wide range of multidimensional chemical and biological assessment operations in a single device, with speed and responsiveness equivalent to their typical lab-based counterparts. Many scholarly researchers have tended treating technical guidance into an available product as a necessity rather than considering the contribution to pursue in areas such as features and functions, sensitivities and low spatial fabrication methods. As a result, it's proposed that lab-on-a-chip researchers focus on inclusion, uniformity, efficiencies for mass-market appeal, and, perhaps most importantly, the device's concept's added value [47].

#### *4.1.1 Innovation in Lab on a chip*

In order for a modern lab-on-a-chip to have a greater chance of commodification and adoption as a routinely used instrument, it must not only outperform existing exact methods in terms of



analysis, price, and usability. If the suggested gadget only provides tiny, incremental advantages for a specific application, end-users may be hesitant to adopt the innovation over more tried ways with well-defined training and data management paths. The 'lab on a chip' concept used for backend operations is not thoroughly understood in some cases. Some systems may be susceptible to building capacity that is not otherwise necessary. Researchers should preferably focus their researches on innovations that are achievable due to the usage of lab-on-a-chip for the maximum degree of business potential and economic benefit of the technology [47].

## 4.2 Microfluidics

Microfluidics is the science and technology of mechanisms that process or manipulate small volumes of fluid ( $10^{-9}$  to  $10^{-18}$  liters) utilizing channels of micrometers in diameter. The first implementations of microfluidic systems were considered, which provides some advantages, including the use of very tiny amounts of samples, as well as high-resolution and sensitivity separations and detections; low cost; quick analysis times; and small footprints for analytical devices [48].

Molecular biology, microelectronics, biodefence, and molecular analysis are four progenitors of the microfluidics area. Then there was the research. Technologies (coupled with the laser's strength in optical detection) allowed for excellent sensitivity and resolution while requiring extremely little quantities. With the success of such micromanaging methods, it seemed only natural to design new, and more adaptable forms for them, as well as explore alternative uses for micro level methods in biochemistry. Microfluidics has witnessed the fast discovery of innovative fabrication processes and microchannels that works as pipes and other structures creating pumps, valves, and mixers, which are critical components of microchemical 'lab on a chip' [49][50][51][52].

Technology revolutions necessitate a diverse spectrum of component and subsystem types, as well as their integration into comprehensive, working systems. Microfluidics is still in its infancy, lacking both of these critical characteristics, as well as the formation of components into systems which is operated by non-experts. The field is in an engrossing phase right now to fascinate scientific community as well as to be developed to meet the expectations. A microfluidic system has a number of common elements, including a way for introducing samples; procedures for mobilizing these fluids through the chip, as well as assembling and mixing them; and several different components. Microfluidics has been able to make use of

several basic differences between the outer characteristics of fluids going through big channels and which are moving through micrometer-scale channels [53] [54].

### ***4.2.1 Applications***

In concept, microfluidic devices have high-value uses, but realizing these applications necessitates advancements in microfluidics; accomplishing two things at the same time is usually challenging. For assuring the development of this field one strategy is the creation of modern types of bioassays for diagnosing patient response to medication; another is the advancements of assays for usage in hospitals. In future, healthcare may shift from treating to preventing sickness. For such anticipatory healthcare, sensitive, regular testing would be required, and microfluidic systems seem to be the most promising technology for such testing [55].

Microfluidics is still in its early stages of development. The research of fluidic cells, the emergence of modern forms of organic fusion in micro-channel systems, the advancement of arrays for detection and high-throughput monitoring, the construction of micro-robotics that use hydrostatics relying on microfluidics, various fluidic editions of MEMS, and a variety of other factors proposes that there are several stage implementations of modules containing fluids. Due to Polydimethylsiloxane's biocompatibility, it may be able to implant microfluidic devices in vivo for some sort of biomedical relevant investigation in the future. Single-molecule studies necessitate tools that can operate with tiny amounts of material, allowing fundamental ideas in cellular biology and molecular biochemistry to be tested. [55]

## **4.3 Microfluidic Devices**

A range of biological assays has been performed using microfluidics with little reagent use. Microfluidics, in particular, have made biological cell tests a popular use due to their small size (10-100  $\mu\text{m}$ ) [56]. Microfluidic engineers have developed a number of other ways for creating submillimeter channels for a variety of reasons, including lower costs, shorter turnaround times, cheaper materials and equipment, and enhanced functionality. These advancements have made it possible to construct microfluidic devices out of a variety of materials and designs, allowing for novel and beneficial physical behaviors and features in microfluidic devices [57]. Microfluidic devices are also known as micro-reactors, lab-on-a-chip, in the literature, depending on their application and characteristics. Microfluidic chips can be made from

various materials using different manufacturing processes, depending on their required function. Because many manufacturing approaches have previously been published in the literature and implemented in reality, the potential for advancements in microfluidics grows rapidly, opening up new opportunities for both academics and industry [58][59]

#### ***4.3.1 Material of Microfluidic Devices***

Plastics remain a prominent alternative in microfluidics due to their many advantageous features and compatibility with biological applications for example, polystyrene is often used for human cell culture. Plastics are low-cost and easily adaptable to high-volume manufacturing processes, making them ideal for those working on commercialization and mass production technologies. Plastics have been regarded as a trustworthy and sturdy medium for these reasons from the early days of microfluidics, even while alternative materials like Polydimethylsiloxane (PDMS) and graphene have grown in popularity [59].

# Chapter 5

## Adaptive Neuro-Fuzzy Inference System (ANFIS)

The simulation results from the COMSOL Multiphysics 5.6 of the microfluidic channels were analyzed using Neuro-Fuzzy Designer toolbox of MATLAB. Pattern of different data can be recognized by a Neural Network on many highly linked processing units. Input data in the form of linguistic variables where different numerical values are expressed in words are used to make decisions in a Fuzzy Logic system. Membership functions are used to create these linguistic variables [60]. Fuzzy Logic system being subjective and heuristic, while Neural Networks contain flaws in their representation of learning. Because the computation of fuzzy rules, inputs, and outputs is reliant on trial and error, designing a fuzzy logic system is time-consuming. The use of Neural Network technology with a Fuzzy Logic system may overcome the limitations of both Neural Networks and Fuzzy Logic systems. A Fuzzy Neural Network is the Adaptive Neuro-Fuzzy Inference System (ANFIS). The main benefit of utilizing ANFIS is that all of its parameters can be trained like a Neural Network inside the framework of Fuzzy Logic system while using both Artificial Neural Networks (ANN) and Fuzzy Logic machine learning techniques. The reasoning process based on Sugeno model, the foundation of the ANFIS model, is shown in **Figure 5.1**[28].

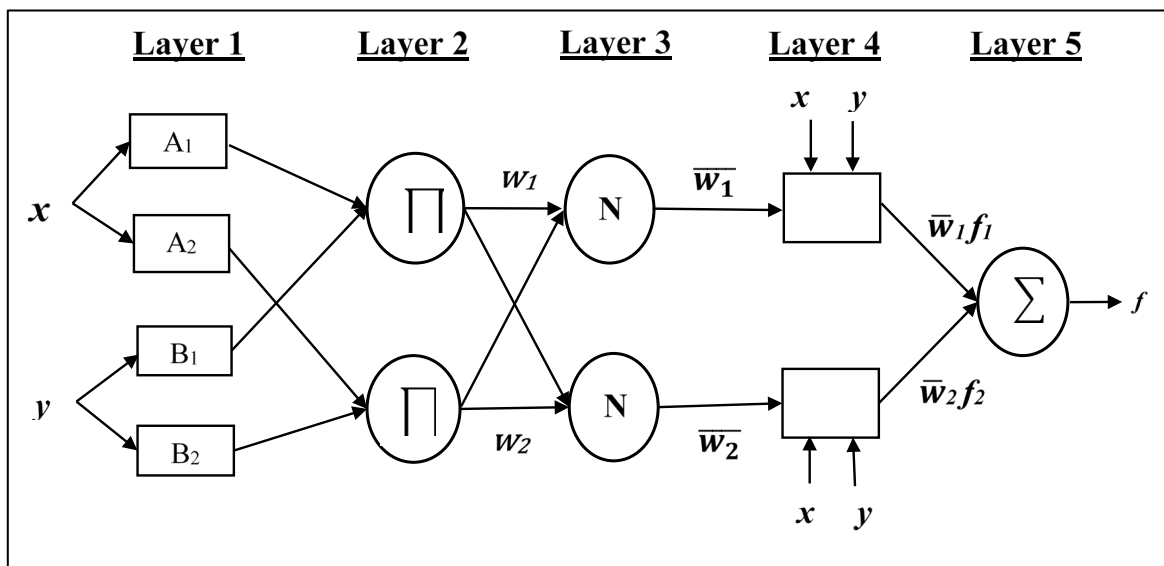


**Figure 5.1:** Five layers of ANFIS architecture with inputs  $x$  and  $y$  [28]

The architecture is made up of five layers in total [28]. Every node  $i$  in layer 1 is a square node. The first layer receives the input values of inlet 2 fluid velocity as  $x$  and electric potentials as  $y$ . This layer determines which membership functions would apply to them. It is also known as the fuzzification layer. In layer 2, every node is labeled as  $\Pi$  where the incoming signals are multiplied and then sends the product as output. The firing strengths for the rules are generated in this layer. Fuzzy operation AND is used in this layer. The firing strength,  $w_i$  is represented by the output of each node.

$$w_i = \mu_{A_i}(x) \times \mu_{B_i}(y), i = 1,2. \quad (5.1)$$

$\mu_{A_i}$  and  $\mu_{B_i}$  are the membership functions of input  $x$  and  $y$  respectively. In layer 3, all nodes are circle nodes labeled  $N$ . The  $i$ th node determines the ratio of the firing strength of the  $i$ th rules to the sum of firing strengths of all rules.

$$\bar{w}_i = \frac{w_i}{w_1 + w_2}, i = 1,2. \quad (5.2)$$

The normalized data  $\bar{w}_i$  and the result parameters are sent into the fourth layer. This layer returns the de-fuzzified values, which are then transferred to the final layer, which returns the final output.

ANFIS has enhanced IF-THEN rules as shown in (5.3) and (5.4) to define the behavior of the whole system without the requirement for previous human experience. The first order Sugeno model is the basis of these two fuzzy rules [28].

$$\text{Rule}_{(1)}: \text{IF } x \text{ is } A_1 \text{ AND } y \text{ is } B_1, \text{ THEN} \quad (5.3)$$

$$f_1 = p_1x + q_1y + r_1.$$

$$\text{Rule}_{(2)}: \text{IF } x \text{ is } A_2 \text{ AND } y \text{ is } B_2, \text{ THEN} \quad (5.4)$$

$$f_2 = p_2x + q_2y + r_2.$$

Here, the inputs are  $x$  and  $y$ .  $A_i$  and  $B_i$  represent fuzzy sets having degrees of membership of inlet 2 fluid velocity parameters and first-phase applied voltage parameters, where  $f_i$  are the outputs within the fuzzy region that have been specified by the fuzzy rules. The design parameters  $p_i$ ,  $q_i$ , and  $r_i$  are established throughout the training procedure.

# Chapter 6

## Methods and Simulation Modelling

### 6.1 Methods

The overview of the whole methodology of this work where two microfluidic channels were proposed and analysis of their performance or the simulation results were also analyzed through Artificial Intelligence, is shown in the following flowchart in **Figure 6.1**. One of the microfluidic channels is intended to separate CTCs from RBCs consisting of two inlets (one for cell mixture and the other for buffer solution) and three outlets. The other microfluidic channel proposed is intended to separate CTCs, RBCs and WBCs consisting of same two inlets with same purpose as the previous type channel and 4 outlets.

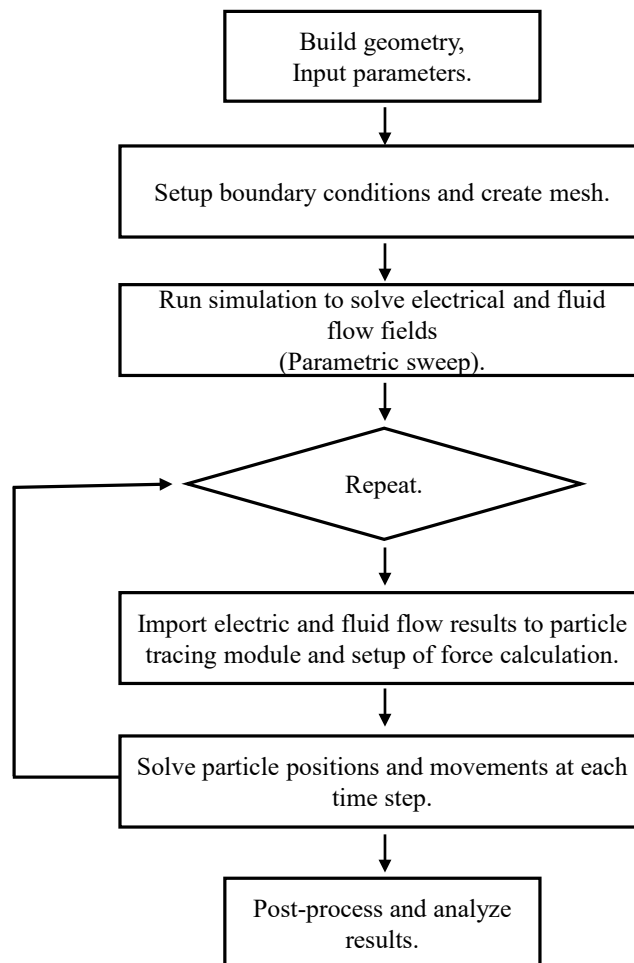
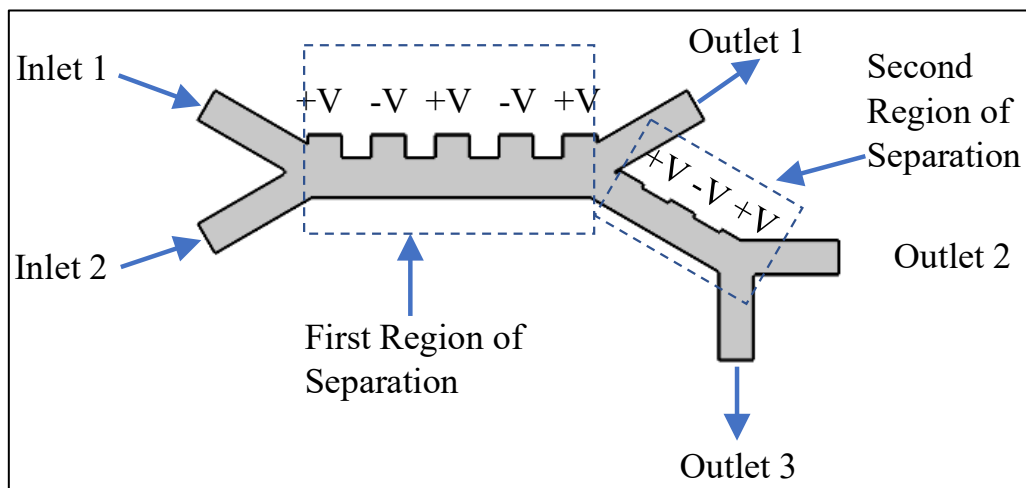


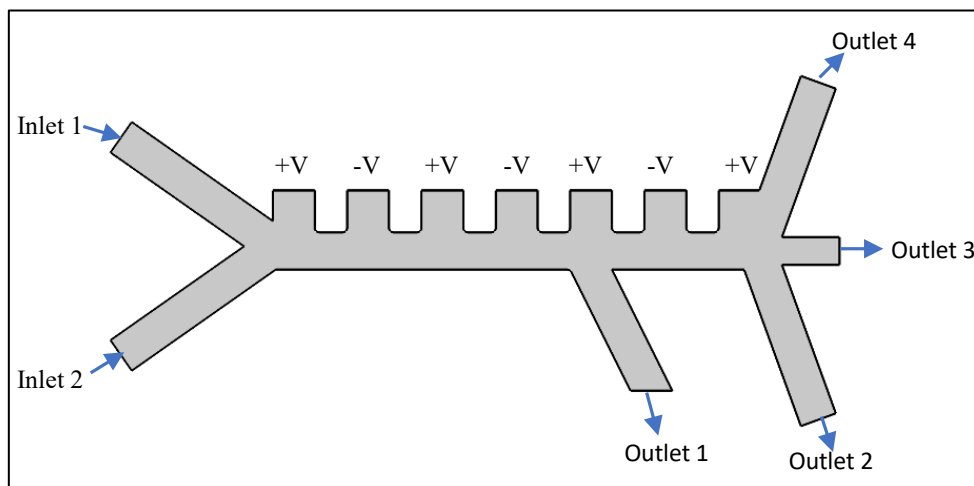
**Figure 6.1:** Flowchart of Simulation

Through inlet 2, buffer solution to alter the velocity distribution and to improve separation process at the outlets, is provided. The proposed channel for separating CTCs from RBCs uses a two-phase separation technique. Outlet 1 is devoted to collect RBCs after the first separation phase. After second-phase separation, outlet 3 collects CTCs whereas, outlet 2 passes the remaining RBCs. The target cells are deflected toward the designated outlets due to the DEP force as well as the extra force from the fluids coming through the inlets provided by the arrangement shown in **Figure 6.2(a)**. On the other hand, the proposed channel for separating CTCs, RBCs and WBCs passes out CTCs through outlet 1, WBCs through outlet 2 and RBCs through outlet 3. Its geometry is shown in **Figure 6.2(b)**.

The initial channel geometry and dimensions were selected from a COMSOL model [33]. However, incorporation of ideas for different applications and techniques led to design the proposed channel structures.



(a)



(b)

**Figure 6.2:** Proposed microfluidic channels

The flow of particles and dielectrophoretic forces imposed on them is evaluated using numerical simulations. The study of a two-dimensional finite element model is proposed and simulated using COMSOL Multiphysics 5.6, which yields the distribution of electric field and flow within the geometry of the channel. Demonstrating the fluid flow using a creeping flow, calculation of the trajectory of CTCs and RBCs under the influence of dielectrophoretic and drag force due to the fluid velocity by tracing particle-fluid flow is done. The equation of drag force on particles flowing with velocity  $v$  is shown below [20]:

$$\overrightarrow{F_{Drag}} = -6\pi Rv, \quad (6.1)$$

Newton's second law of motions was followed by the particles with equation governed by force and momentum. The equation of particle motion of a cell of mass  $m_{cell}$  is expressed as [20]:

$$m_{cell} \left( \frac{\partial v}{\partial t} \right) = \overrightarrow{F_{DEP}} + \overrightarrow{F_{Drag}} = \overrightarrow{F_{cell}}, \quad (6.2)$$

here  $\overrightarrow{F_{cell}}$  is the total force acting on the particles. The electric field distribution from the electrodes and their different arrangements in the channels are also evaluated in this study to bring out the optimized structures of the channel.

## 6.2 Simulation Modeling

The Electrostatic field equations govern the electric field distribution inside the microchannel under steady-state circumstances. Keeping the electric potential of the electrodes constant and the inlets, outlets, and wall surface of the microchannel boundary conditions insulated in COMSOL, the electric field of the microchannel is controlled by following equations [44],

$$\nabla \cdot j = Q_i, \quad (6.3)$$

$$J = \sigma E + J_e, \quad (6.4)$$

$$E = -\nabla V, \quad (6.5)$$



The boundary condition of the channel wall is non-slip boundary for controlling the flow. Due to the small value of Reynolds number, the inertial forces are less in comparison with the viscous forces. Hence, the inertial term can be omitted in the Navier-Stokes equations for this study as shown in (6.6). So, the Electrostatic field equations of the Stokes flow to convert momentum and the continuity equation to convert mass are applied as [44],

$$\nabla \cdot [-pI + \mu(\nabla u + (\nabla u)^T)] + F = 0, \quad (6.6)$$

$$\rho \nabla \cdot (u) = 0 \quad (6.7)$$

### 6.3 Material and Properties

The particle movements are tracked by the particle trajectory module in COMSOL. The modeling of the particles is done considering their electrical and geometrical properties shown in **Table 6.1**. The dielectric characteristics of a cell is dependent on the cell diameter. For not choosing proper equivalent structure of the cells, misleading and unintended simulation results might be obtained [30].

Because cells are made up of nucleus, cytoplasm, and cell membranes with varying electrical characteristics, most particles are complicated and heterogeneous. As a result, the single-shell model may be expanded to the multi-shell model to properly describe heterogeneous architectures of the cells. Erythrocytes, for example, may be represented using a single-shell model. Modeling of leukocytes with nuclei, on the other hand, necessitates a three-shell model, with three distinct shells representing the plasma membrane, cytoplasm, and membrane that covers the nucleoplasm [61].

Some cells may be comparable to a solid sphere, while others need the development of a biological particle equivalent model. The concentric spherical model is the most popular among them. The effective dielectric constant ( $\epsilon_{eq}^*$ ) of a single spherical model is given below [21]:

$$\epsilon_{eq}^* = \epsilon_s^* \frac{\left(\frac{r_0}{r_i}\right)^3 + \frac{2(\epsilon_p^* - \epsilon_s^*)}{\epsilon_p^* + 2\epsilon_s^*}}{\left(\frac{r_0}{r_i}\right)^3 - \frac{2(\epsilon_p^* - \epsilon_s^*)}{\epsilon_p^* + 2\epsilon_s^*}}, \quad (6.8)$$

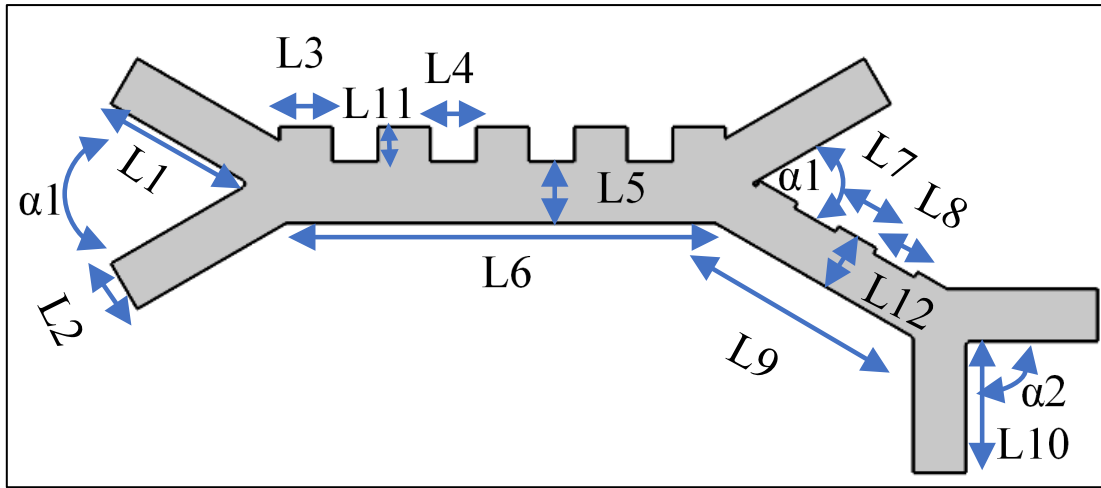
the parameter  $\epsilon_s^*$  in the aforementioned equation is the complex permittivity of the outer shell,  $r_i$  is the inner radii, and  $r_o$  is the outer radii of the shell. To achieve the goal of the separation of the CTCs from other blood cells using an optimized microfluidic channel, valid dielectric, electric and structural characteristics of the particles as well as the buffer medium are taken, which is shown in **Table 6.1**[3], [62]

**Table 6.1** Electrical and Flow Properties of Elements of the Simulation

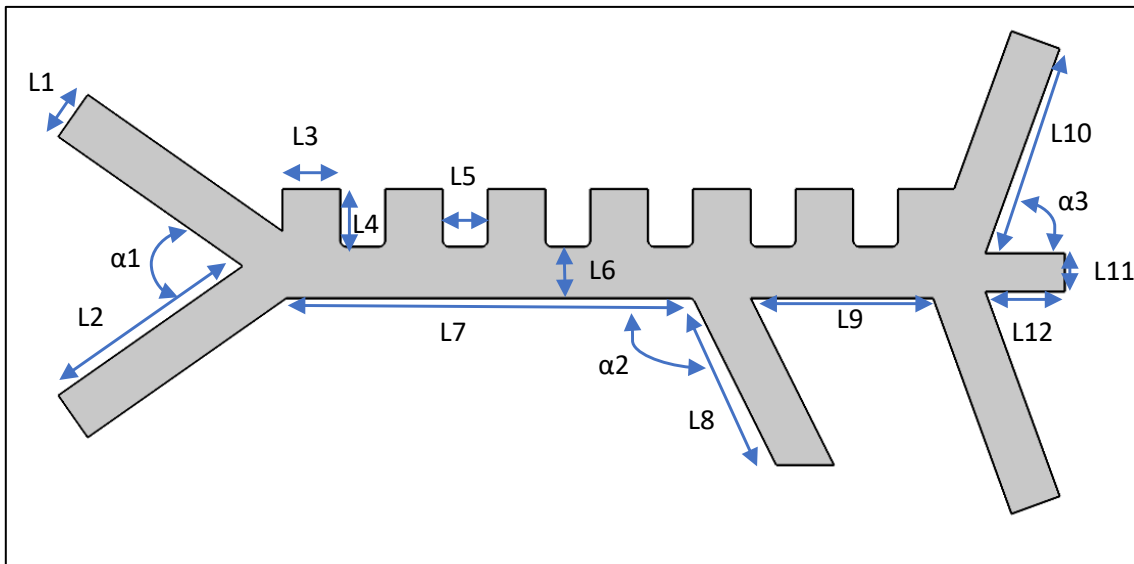
<b>Parameters (units)</b>	<b>Medium</b>	<b>RBC</b>	<b>CTC</b>	<b>WBC</b>
<b>Density (<math>kg/m^3</math>)</b>	1000	1050	1050	1050
<b>Diameter (<math>\mu m</math>)</b>	-	5	12	9.4
<b>Conductivity (<math>S/m</math>)</b>	0.055	0.31	0.62	0.487
<b>Particle Relative Permittivity</b>	80	59	130	136
<b>Shell thickness of the particle (nm)</b>	-	9	9	6.5
<b>Shell conductivity (<math>\mu S/m</math>)</b>	-	1	1	7.25
<b>Shell Relative permittivity</b>	-	4.44	4.44	10.3

## 6.4 Modeling and Geometry

The layouts of the microfluidic channels are shown in **Figure 6.3(a)** and **Figure 6.3(b)** respectively.



(a)



(b)

**Figure 6.3:** Layouts of the proposed microfluidic channels with labeling for showing dimensions.

The angles and dimensions of different parts of **Figure 6.3(a)** and **Figure 6.3(b)** are defined in **Table 6.2** and **Table 6.3**.

**Table 6.2** Dimensions of the Microfluidic channel of **Figure 6.3(a)**

Parameter	Symbol	Value
Inlet channel length	L1	182 $\mu$ m
Inlet-outlet channel width	L2	60 $\mu$ m
Electrode slot length (first region)	L3	60 $\mu$ m
Length between slots (first region)	L4	52 $\mu$ m
Width of the separation regions	L5	70 $\mu$ m
Length of first region of separation	L6	490 $\mu$ m
Electrode slot length (second region)	L7	50 $\mu$ m
Length between slots (second region)	L8	54 $\mu$ m
Length of second region of separation	L9	260 $\mu$ m
Outlet channel length	L10	150 $\mu$ m
Electrode slot height (first region)	L11	40 $\mu$ m
Second region width with electrode	L12	67 $\mu$ m
Angle between inlet 1 and 2	$\alpha$ 1	30 degrees
Angle between outlet 1 and second region of separation	$\alpha$ 1	30 degrees
Angle between outlet 2 and 3	$\alpha$ 2	90 degrees

**Table 6.3** Dimensions of the Microfluidic channel of **Figure 6.3(b)**

Symbol	Value
L1	40 $\mu$ m
L2	175 $\mu$ m
L3	45 $\mu$ m
L4	40 $\mu$ m
L5	35 $\mu$ m
L6	40 $\mu$ m
L7	314 $\mu$ m
L8	142 $\mu$ m
L9	142 $\mu$ m
L10	170 $\mu$ m
L11	30 $\mu$ m
L12	62 $\mu$ m
$\alpha$ 1	30 degrees
$\alpha$ 2	120 degrees
$\alpha$ 3	70 degrees

These dimensions are achieved after intense modelling and simulations to bring out the maximum separation result for the CTCs from different blood cells. However, analysis of the simulations results through ANFIS guided for specific inputs that should be provided to achieve any specific output through these microfluidic channels.

# Chapter 7

## Results

The channel for separating CTCs from RBCs and also the channel for separating CTCs from WBCs and RBCs were simulated and observed in COMSOL. Three studies were performed and simulated in COMSOL and the results were observed individually for both the channels.

### 7.1 Results from the Channel for Separating CTCs from RBCs

#### 7.1.1 Mesh Analysis of the Channel

In modern technology, modeling and testing need the use of Finite Element Method (FEM). The goal of the FEM model is to separate the CTCs from RBCs in the proposed microfluidic channel using COMSOL's physics-controlled mesh with element size 'normal' where the number of mesh vertices is 2917 and number of elements is 4961 shown in **Figure 7.1**.

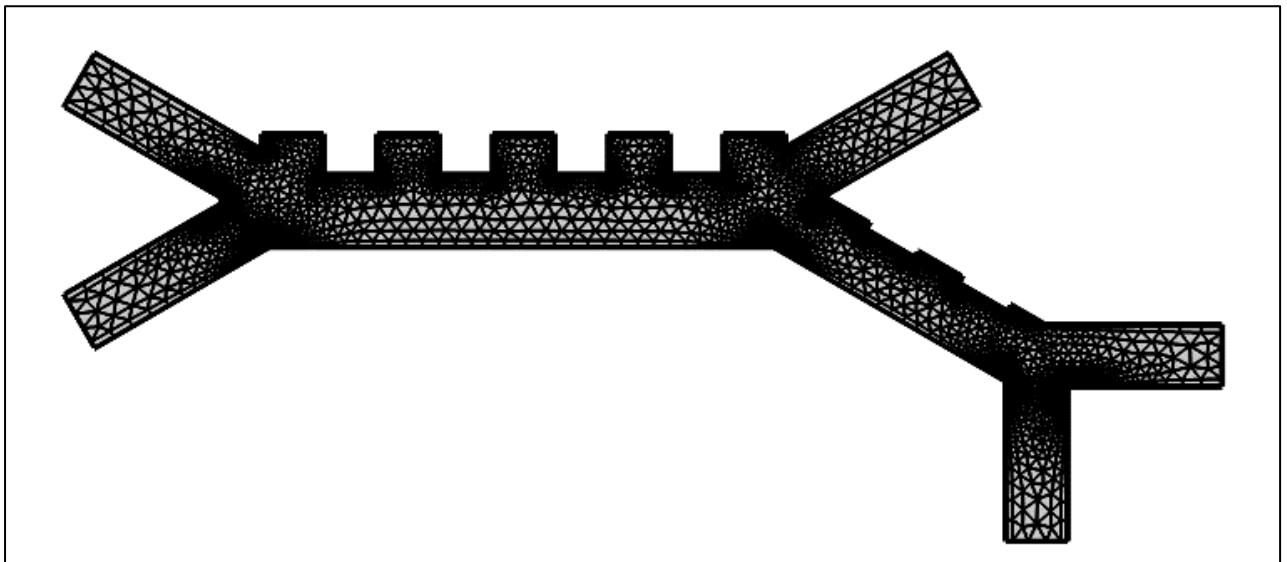


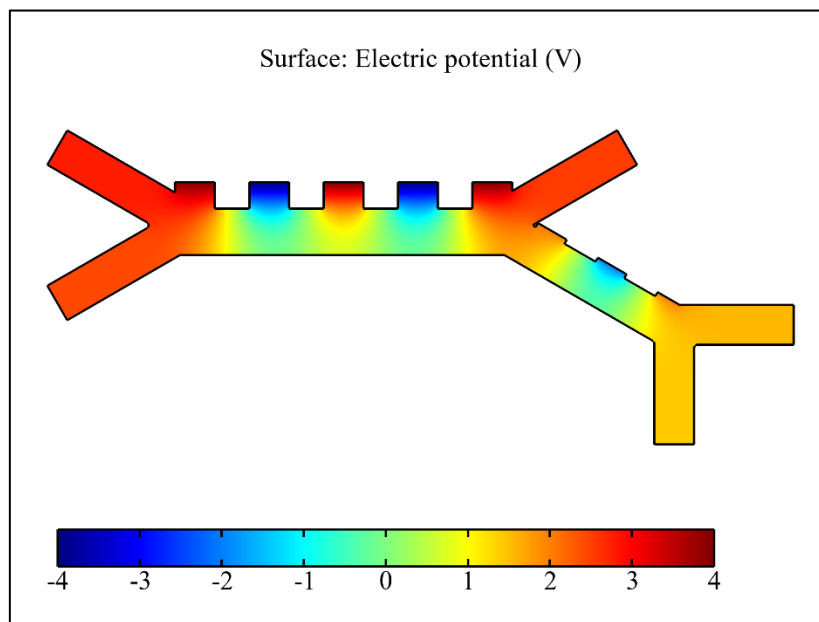
**Figure 7.1:** The two-dimensional meshed model of the dielectrophoretic separation channel which separates CTCs from RBCs

The purpose of mesh analysis is to divide the model into small segments in order to solve the model at discrete points in space and getting the results easily. The greater the number of mesh

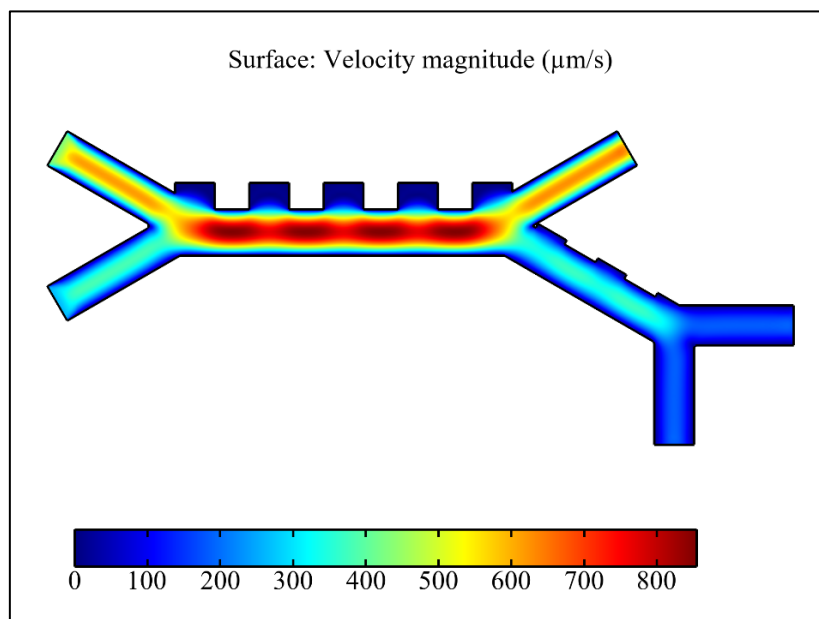
elements the lesser error will result at the cost of greater computing power and time. So, an optimal mesh size is to be selected depending on the model.

### 7.1.2 Results from Study 1

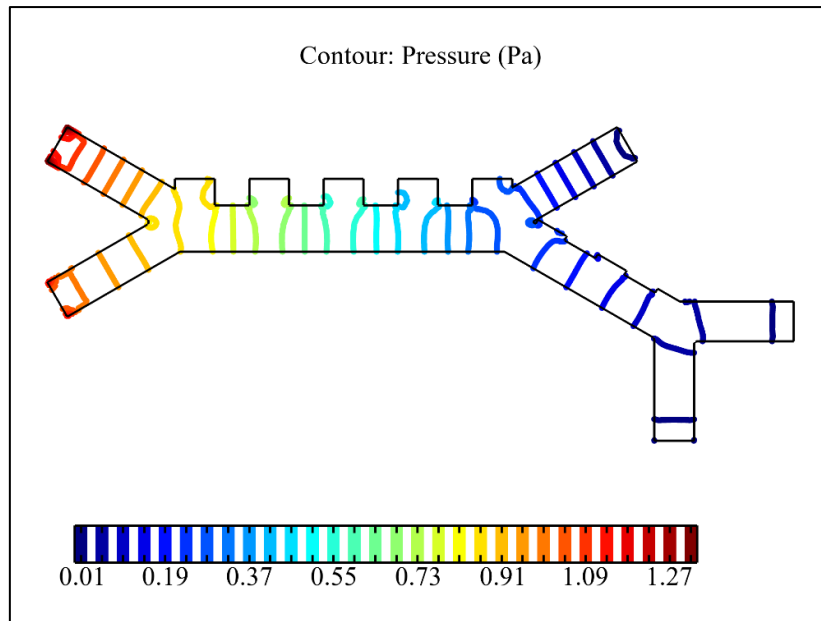
This study solves for the velocity magnitude, pressure, and AC electric potential. The outcomes of this study are shown in **Figure 7.2(a), (b) and (c)**.



(a)



(b)



(c)

**Figure 7.2:** Spatial variation of (a) surface electric potential (V), (b) velocity ( $\mu\text{m/s}$ ), and (c) pressure (Pa)

### 7.1.3 Results from Study 2

Study 2 estimates the particle trajectories in the flow without application of any electric field which means, no DEP force will act on the particles, so that all particles (CTCs and RBCs) follow the same path. The observed result is shown in **Figure 7.3**. The CTCs and RBCs mixture velocity at the upper inlet (inlet 1) was kept fixed at  $420 \mu\text{m/s}$  and the buffer fluid (deionized water) velocity at the lower inlet (inlet 2) was kept fixed at  $260 \mu\text{m/s}$ .

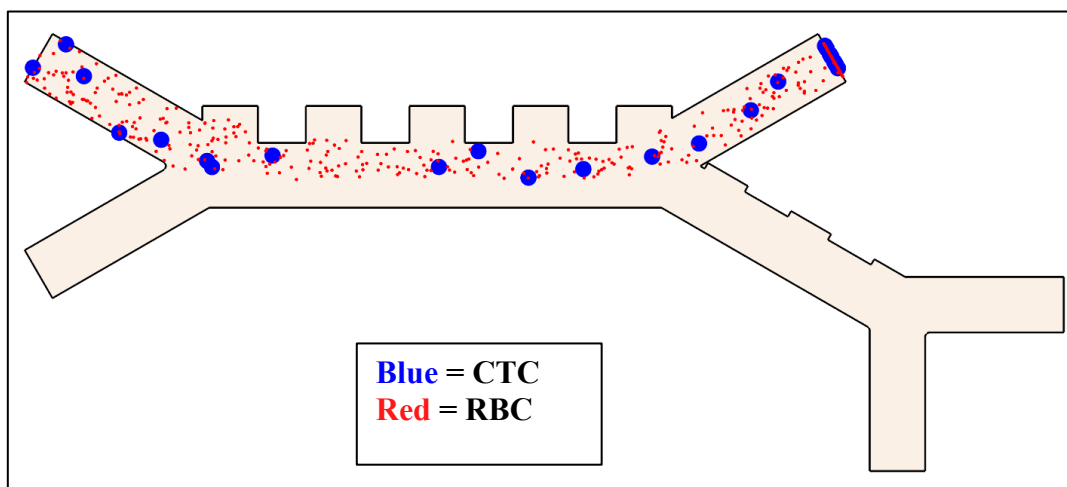


**Figure 7.3:** Particle Trajectories without application of any electric field

Here in **Figure 7.3** the blue dots represent CTCs and the red dots represent RBCs. It can be seen that as there is no electric field applied there is no formation of DEP force as a result of which all the particles follow the same path and move out through the same outlet.

#### **7.1.4 Results from Study 3**

Study 3 estimates the particle trajectories in the flow after application of electric field which means, DEP force will act on the particles, as a result of which different particles follow different path depending on the force, they experience which is proportional to the diameter of the particle itself. The observed result is shown in **Figure 7.4**. Here the applied electric field was 8V peak-to-peak with the CTCs and RBCs mixture velocity at the upper inlet (inlet 1) was kept fixed at  $420 \mu\text{m/s}$  and the buffer fluid (deionized water) velocity at the lower inlet (inlet 2) was kept fixed at  $260 \mu\text{m/s}$ .

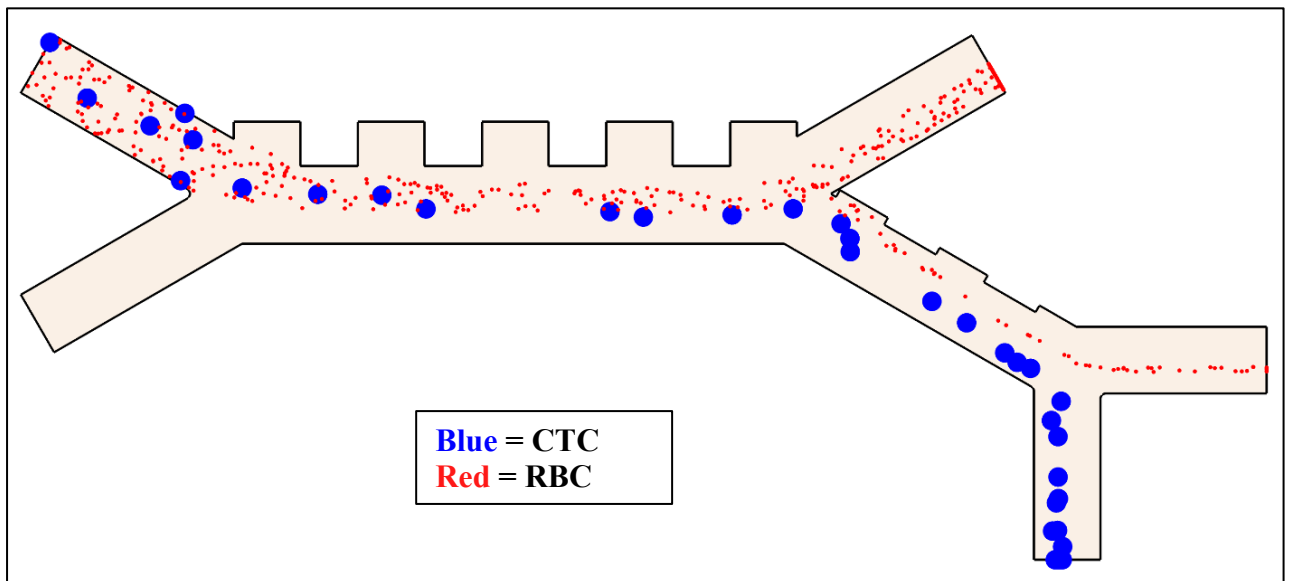


**Figure 7.4:** Particle Trajectories after application of non-uniform electric field (8V peak-to-peak)



### 7.1.5 Effect of Shape and Design variation of the Microfluidic Channel on the Results of Study 3

Initial simulation was carried out with single phase separation where outlet 1 was assigned to flow RBCs and the outlet 2 was assigned to flow CTCs. The figure of the microfluidic channel having single phase separation with electrode arrangement is shown in **Figure 7.5**.

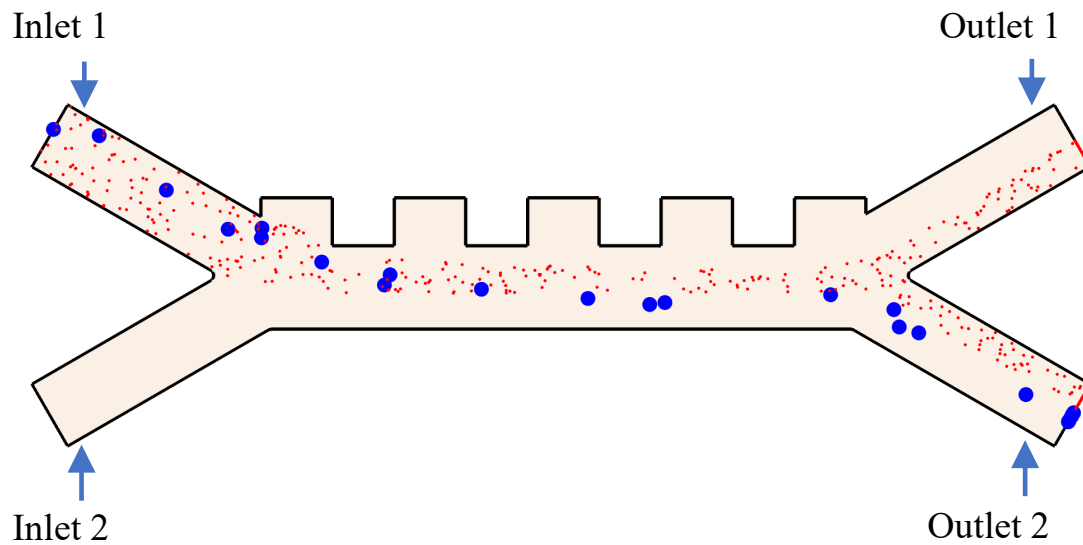
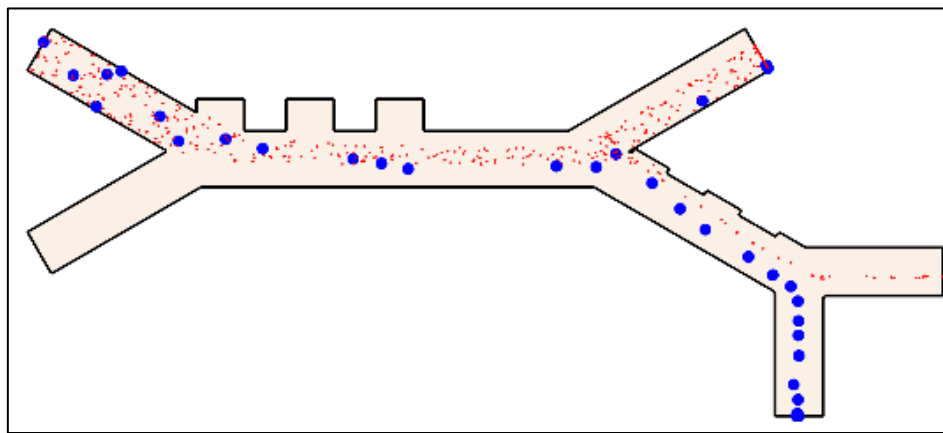


**Figure 7.5:** Particle trajectories for single phase separation model where separation failed at 8 V peak-to-peak applied voltage and  $420\mu\text{m/s}$  inlet 1 fluid velocity and  $260\mu\text{m/s}$  inlet 2 fluid velocity

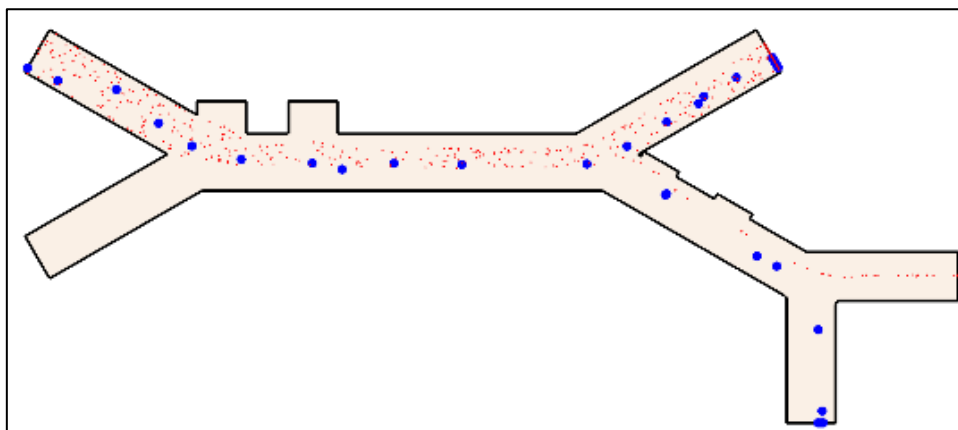
However, it has been observed that the structure in **Figure 7.5** couldn't separate the particles properly. Some RBCs were flowing with CTCs through outlet 2. This failure to separate CTCs from RBCs which can be seen **Figure 7.5** was due to the lack of the enough DEP force that could further isolate the particles at the outlet 2. So, a two-phase separation technique where the outlet 2 of **Figure 7.5** was extended with additional electrodes placed to form a second-phase separation region with an additional outlet for getting enough DEP force to separate the particles, has been adopted. In this study, 802 RBC particles mixed with 41 CTC particles were passed through inlet 1 of the microfluidic channel for a clearer view of CTCs being separated from a huge number of RBCs in a shorter simulation time.

### 7.1.6 Effect of Variation of Number of Electrodes of the Microfluidic Channel on the Results of Study 3

The simulation results of the effect of electrode number in separation of the particle are shown in **Figure 7.6**. It is seen from **Figure 7.6(a)** that there are three electrodes placed in both the first and second regions of separation and in **Figure 7.6(b)** two electrodes were placed in both the first and second regions of separation of the microfluidic channel. However, both of these channels failed to separate CTCs from RBCs fully. This occurred due to lesser number of electrodes. As the amount of electric field produced by the electrodes depend on the number of electrodes, these two microfluidic channels of **Figure 7.6** were unable to generate enough DEP force on the particles.



(a)



(b)

**Figure 7.6:** Schematic and particle trajectories of the microfluidic channels having 8V peak-to-peak at the first region of separation electrodes failing to separate having (a) 3 electrodes in the first separation region and 3 electrodes in the second separation region; (b) 2 electrodes in the first separation region and 2 electrodes in the second separation region.

Electric field gradient that is produced at the edges of the electrode blocks when an electric potential is applied on them, results in the production of DEP forces. A lower voltage would be utilized if the cell diameters are large. For the separation of cells with a small diameter, however, a greater voltage should be employed [63].

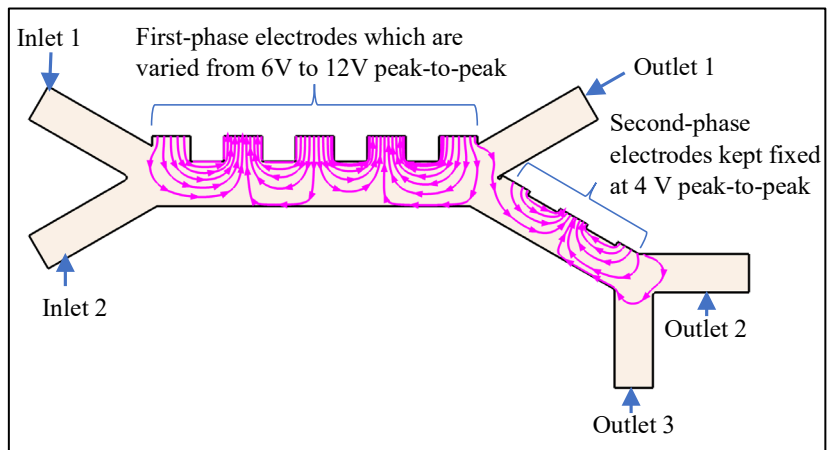
Due to the applied AC signal of 100 kHz on the electrodes of the microfluidic channel both the particles respond to nDEP force and deviate from the electrodes.  $4\pi r_p^3$  in (3.3) functioning as a shape factor. There is a relation between DEP force that a particle is exposed to and a particle's diameter in (3.4). Simulation results showed that the particles with larger diameter experienced more DEP force and deviated more from the electrode. CTCs having larger diameter of 12 $\mu\text{m}$  than the diameter of RBCs of 5  $\mu\text{m}$  tend to deviate more from the electrodes than RBCs.

### ***7.1.7 Effect of Variation of Electric Potential of Electrodes of the Microfluidic Channel on the Results of Study 3***

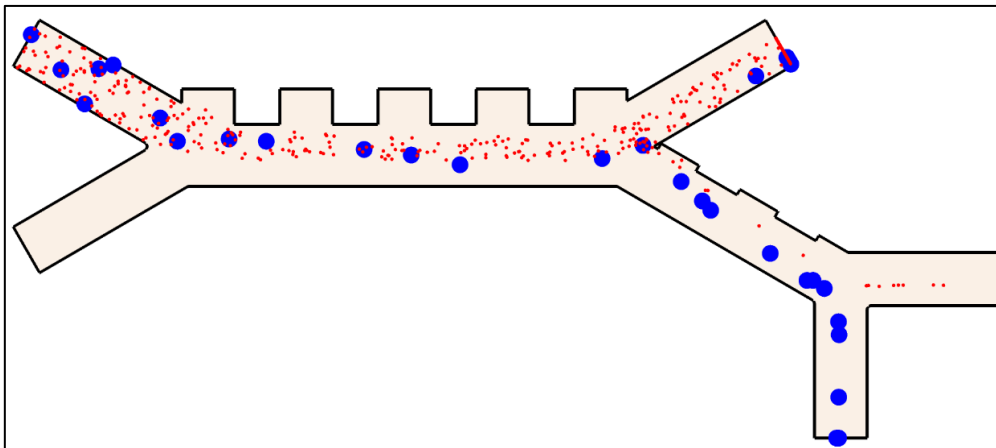
Influence of the applied voltage on particle movement in the microfluidic channel having 5 electrodes in the first separation region and 3 electrodes in the second separation region is shown in **Figure 7.7**. The electric field distribution is shown in **Figure 7.7(a)**. When a peak-to-peak voltage of 6 V is applied on the electrodes at the first-phase separation region keeping 4V peak-to-peak applied voltage at the second phase electrodes, the simulation result showed that the DEP force was not strong enough to pass all the CTCs towards the second-phase separation region which can be seen in **Figure 7.7(b)**. Few CTCs passed through outlet 1 which was supposed to be the pathway for RBCs. In **Figure 7.7(d)**, for 10 V peak-to-peak applied voltage at the first-phase electrodes keeping 4V peak-to-peak applied voltage at the second phase electrodes and in **Figure 7.7(e)**, for 12 V peak-to-peak applied voltage at the first-phase electrodes keeping 4V peak-to-peak applied voltage at the second phase electrodes, larger DEP forces were pushing CTCs towards the microfluidic channel wall excessively which caused some of the CTCs to get stuck at the microfluidic channel wall and thus, clogging of the particles was observed. Also, Joule heating effect can cause cell damage if excessive voltage is applied [64].

However, for 8 V peak-to-peak applied voltage at the first-phase electrodes keeping 4V peak-to-peak applied voltage at the second phase electrodes, expected separation was observed in

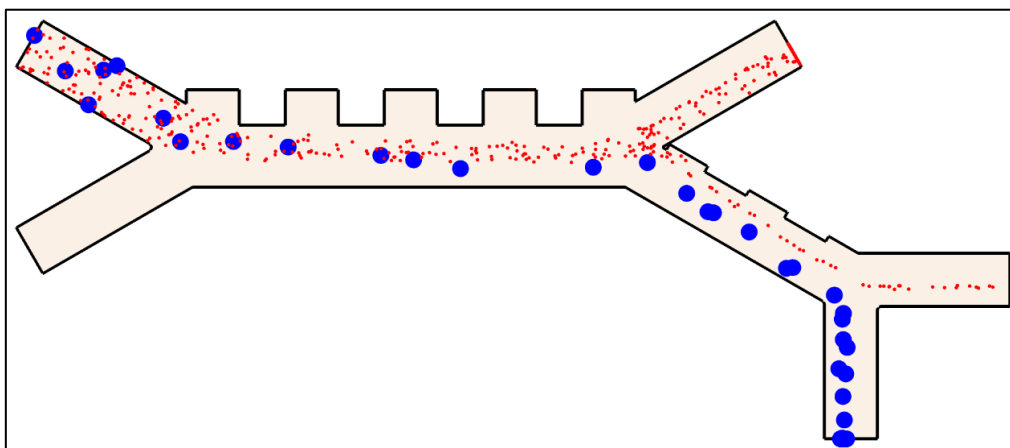
**Figure 7.7(c)** where RBCs passed through outlet 1 and outlet 2 and the CTCs passed through outlet 3 without any kind of clogging.



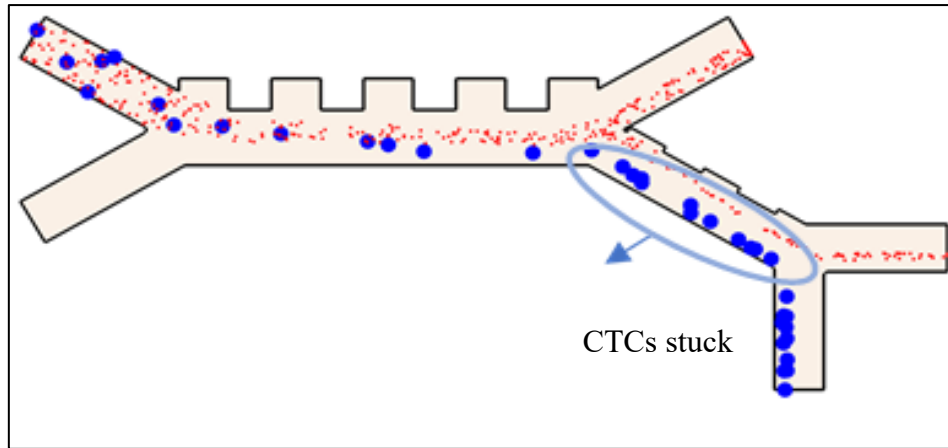
(a)



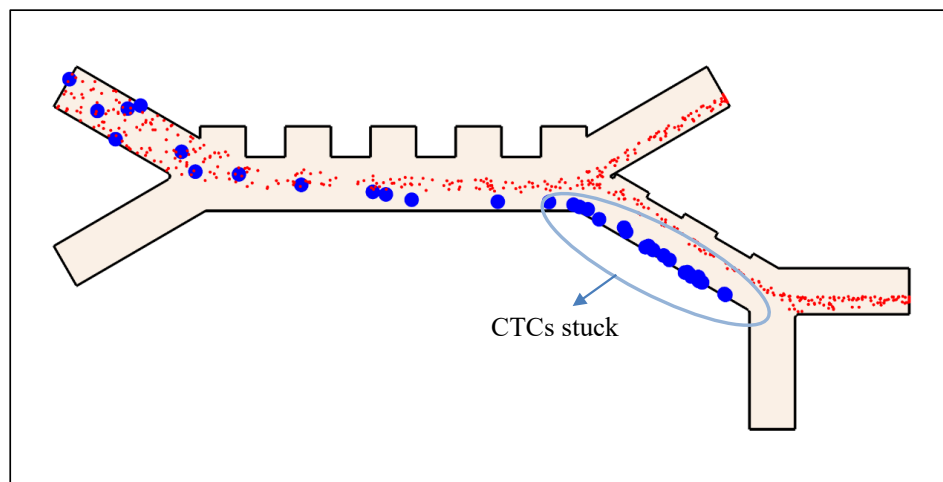
(b)



(c)



(d)



(e)

**Figure 7.7:** (a) Electric field distribution due to the applied voltages, simulation results of particle trajectories with  $420\mu\text{m/s}$  inlet 1 fluid velocity and  $260\mu\text{m/s}$  inlet 2 fluid velocity at (b) 6V peak-to-peak applied voltage at first phase electrodes and 4V peak-to-peak applied voltage at the second phase electrodes, (c) 8V peak-to-peak applied voltage at first phase electrodes and 4V peak-to-peak applied voltage at the second phase electrodes, (d) 10V peak-to-peak applied voltage at first phase electrodes and 4V peak-to-peak applied voltage at the second phase electrodes, and (e) 12V peak-to-peak applied voltage at first phase electrodes and 4V peak-to-peak applied voltage at the second phase electrodes.

### 7.1.8 Analysis of the Results from Simulation of the Microfluidic Channel using ANFIS

The following data in **Table 7.1** were obtained from simulation of the microfluidic channel in COMSOL. Here the distribution values 1, 3, and 5 represent no separation, separation after second-phase separation region, and separation before second-phase separation region of the CTCs respectively.

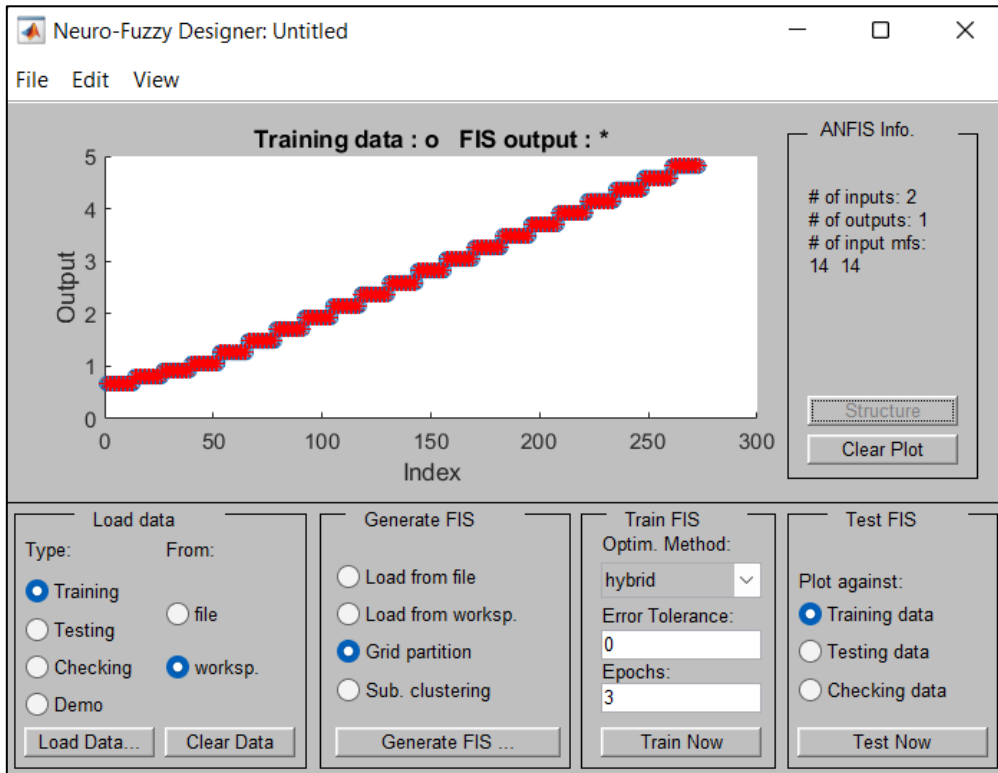
**Table 7.1** Obtained Outputs with Respect to Inputs in COMSOL

Inlet 2 Velocity ( $\mu\text{m/s}$ )	Voltage (V)	Distribution	Pressure (Pa)	Outlet 3 Velocity ( $\mu\text{m/s}$ )
0-150	0-10	1	1.01-1.20	111-151
200	4	3	1.26	165
250	4-5	3	1.32	178
300	4-6	3	1.38	191
350	4	5	1.45	205
350	5-6	3	1.45	205
400	4-5	5	1.51	218
400	6	3	1.51	218
450	4-5	5	1.61	231
450	6-7	3	1.61	231
500	4-6	5	1.73	244
500	7	3	1.73	244
550	5-6	5	1.85	258
550	7	3	1.85	258
600-650	5-7	5	1.97	271
601-650	8	3	1.97	271
700-800	5-8	5	2.21-2.46	297-324
850-1000	5-9	5	2.58-2.94	337-377

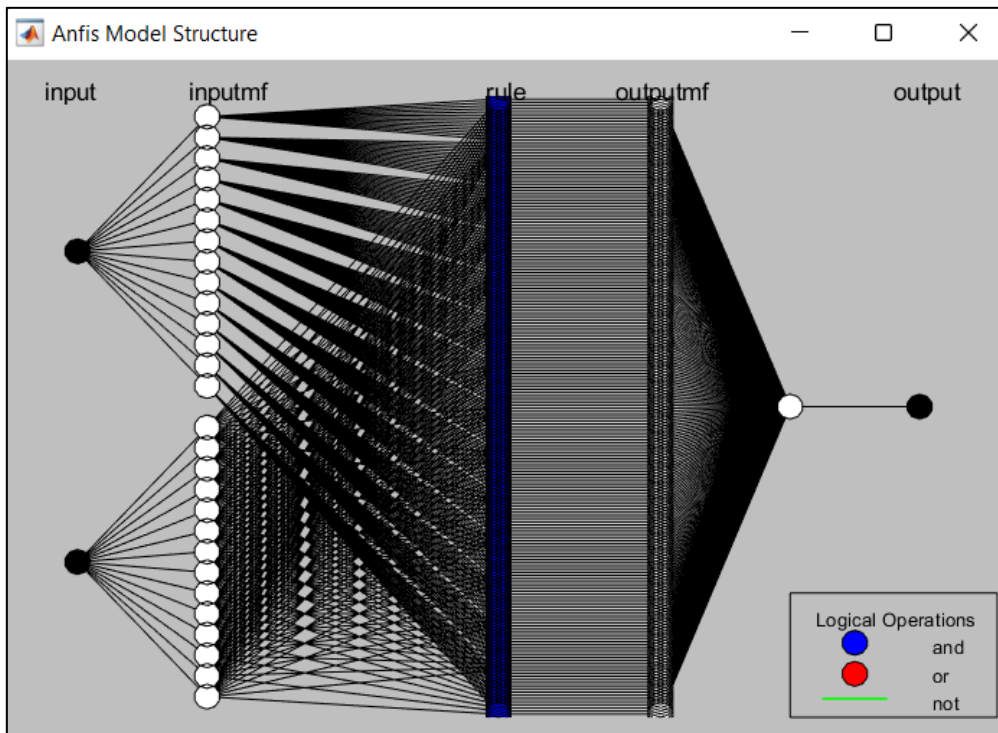
In the neuro-fuzzy toolbox of MATLAB the following data were fed:

- Buffer fluid velocity at inlet 2 and electric potential given as inputs.
- Maximum pressure, outlet 2 velocity and distribution of the particles given as outputs.

The data from **Table 7.1** were fed to the Neuro-Fuzzy Designer of MATLAB as shown in **Figure 7.8(a)**. For both inputs, 14 membership function were chosen in Neuro-Fuzzy Designer toolbox of MATLAB for this study that leads to the generation of 196 fuzzy rules. The ANFIS model structure has been shown in **Figure 7.8(b)**.



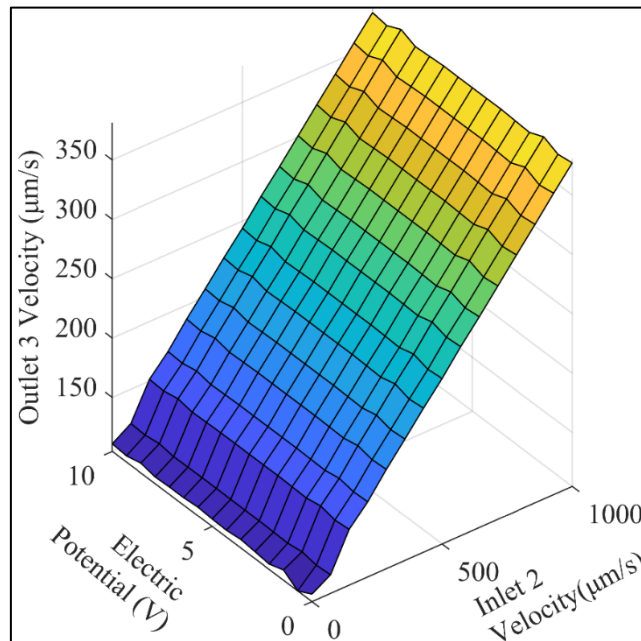
(a)



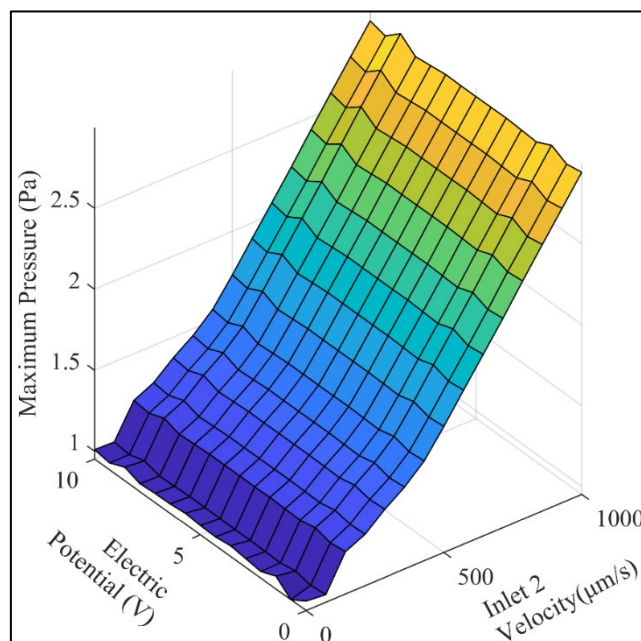
(b)

**Figure 7.8:** (a) Neuro-Fuzzy Designer, and (b) ANFIS model structure

ANFIS utilizes the neural network to train all its parameters within the structure of the Fuzzy Logic system. Though the training process Neuro-Fuzzy Designer predicts outputs for different inputs given to the system. Increasing the number of membership functions of the input increases accuracy but sacrifices more computing power and time required for computation. 90% of the data was used for training and 10% was used for testing and RMSE was found to be 0.48. The following figures were generated as given in **Figure 7.9**.

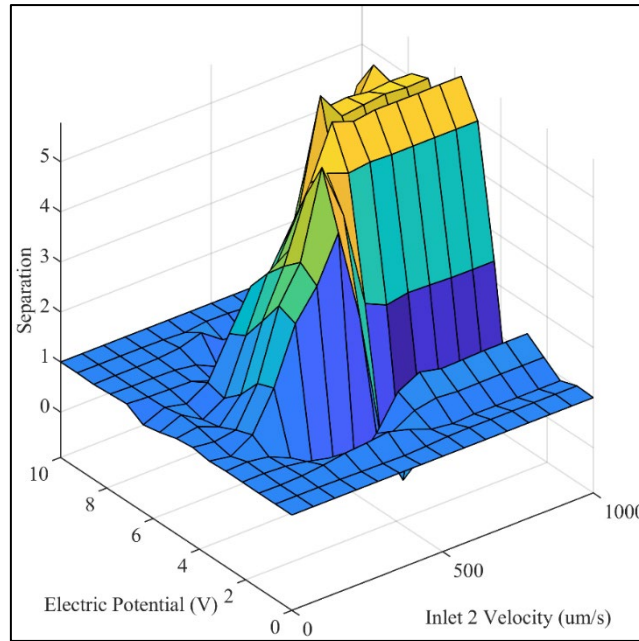


(a)



(b)





(c)

**Figure 7.9:** Effect of the fluid velocity at inlet 2 and electric potential of the electrodes on (a) outlet 3 fluid velocity ( $\mu\text{m/s}$ ), (b) maximum pressure (Pa) on the microfluidic channel, and (c) separation of CTCs and RBCs

The Neuro-Fuzzy Designer resulted three 3D graphics that shows the relationship between input and output parameters with the help of neural network prediction and fuzzy logic rules. **Figure 7.9(a)** and **Figure 7.9(b)** shows the fluid velocity of the buffer fluid at inlet 2 effecting the outlet 3 velocity and maximum pressure in the microfluidic channel linearly. However, the effect of the highest electric potentials of the electrodes on the outlet 3 velocity and maximum pressure in the microfluidic chip is less. In **Figure 7.9(c)**, the effect of fluid velocity of inlet 2 over the separation profile of the CTCs is non-linear. The effect of the highest electric potentials of the electrodes on the separation profile is also non-linear.

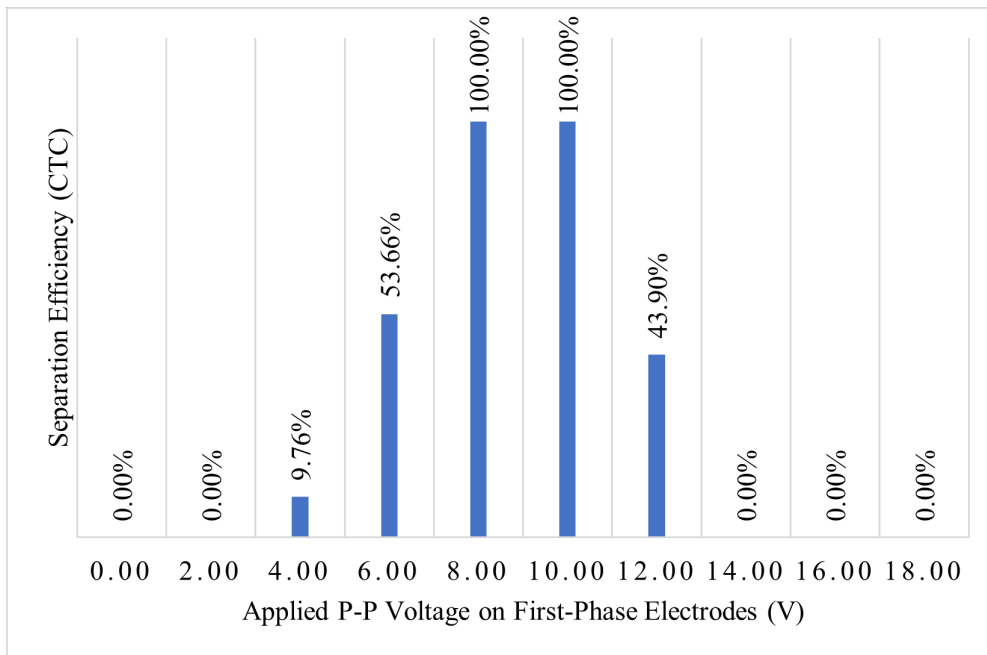
### 7.1.9 Separation Efficiency (SE) and Separation Purity (SP) of the Microfluidic Channel

As the force due to DEP is a function of the amplitude of the applied voltage. The effect due to different applied voltage on the movement of the particle is clearly observable. Different voltage values have given different results for particle movement trajectory. The microfluidic channel that has been modeled in this work showed 100 percent separation efficiency (SE) and separation purity (SP) for 8 V peak-to-peak applied voltage at the first-phase separation region and 4 V peak-to-peak at the second-phase separation region. The SE and SP are used to evaluate the performance of the microfluidic channel [29]. Mathematical expression of SE and SP are expressed in (7.1) and (7.2) respectively.

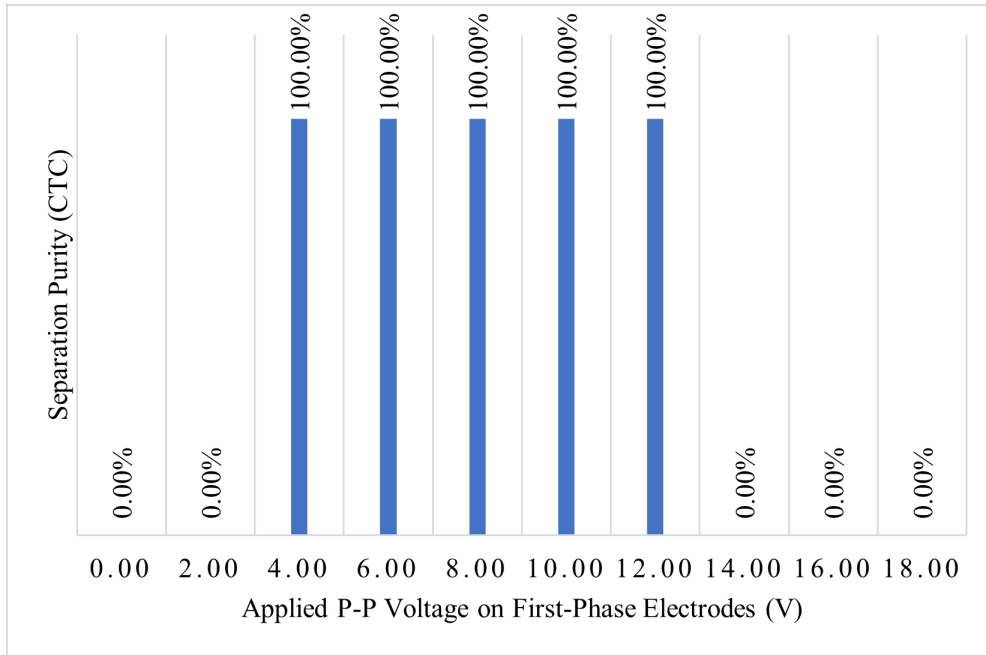
$$SE(CTC) = \frac{\text{Number of CTCs at outlet 3}}{\text{Number of CTCs at inlet 1}} \quad (7.1)$$

$$SP(CTC) = \frac{\text{Number of CTCs at outlet 3}}{\text{Number of CTCs and RBCs at outlet 3}} \quad (7.2)$$

The total number of CTCs and RBCs given as input into the channel were 41 and 802 respectively. **Figure 7.10** depicts the performance metrics as SE and SP of the microfluidic channel with applied voltage on the first-phase region electrodes.



(a)



(b)

**Figure 7.10:** Variation of (a) SE, and (b) SP of CTC with respect to applied peak-to-peak voltage on the first-phase electrodes (Keeping Inlet 1 velocity - 420um/s, Inlet 2 velocity - 260um/s, 2nd phase electrodes 4 V Peak-to-Peak as fixed quantities)

**Figure 7.10(a)** shows that the SE of the microfluidic channel starts increasing from 4V peak-to-peak applied voltage on the electrodes at the first-phase separation region keeping 4V peak-to-peak applied voltage at the second phase electrodes and achieves 100 percent SE for 8V and 10V peak-to-peak applied on the electrodes at the first-phase separation region keeping 4V peak-to-peak applied voltage at the second phase electrodes. Further increasing the voltage causes the SE to decrease due to clogging of the CTCs inside the microfluidic channel. **Figure 7.10(b)** shows 100 percent SP is achieved for 4V to 12V peak-to-peak applied voltage on the electrodes at the first-phase separation region keeping 4V peak-to-peak applied voltage at the second phase electrodes.

## 7.2 Results of the channel for separating CTCs from WBCs and RBCs

### 7.2.1 Mesh Analysis of the Channel

The physics-controlled meshed model of the microfluidic channel which separates CTCs from WBCs and RBCs having the number of mesh vertices is 3838 and number of elements is 6553 for precise simulation results is shown in **Figure 7.11**.

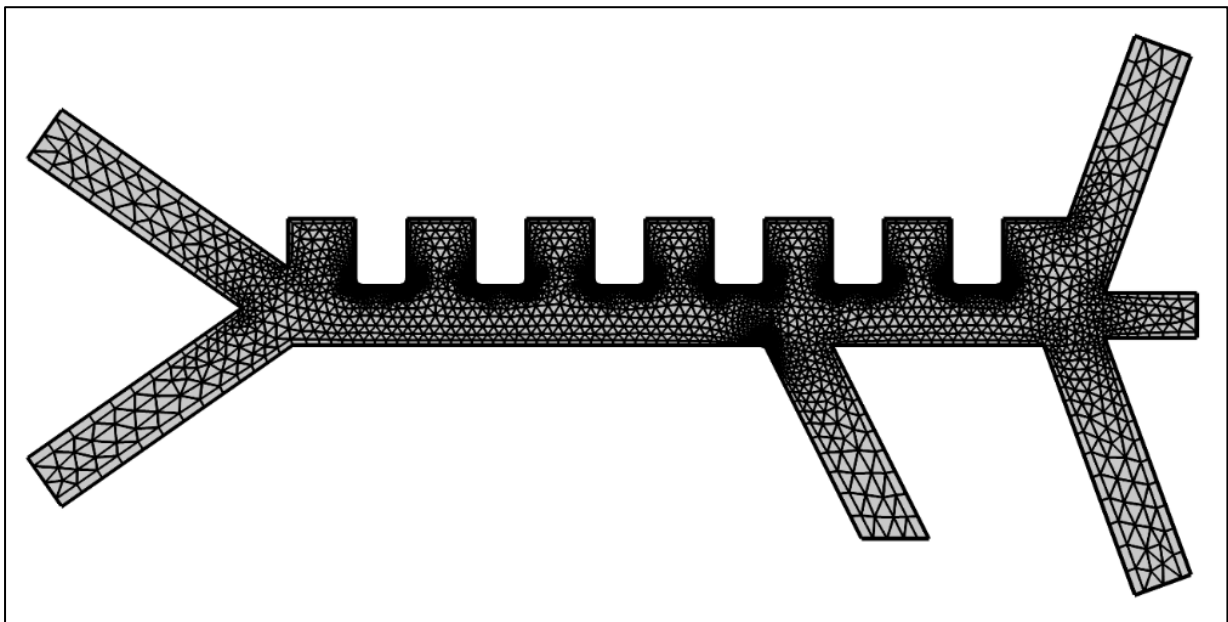
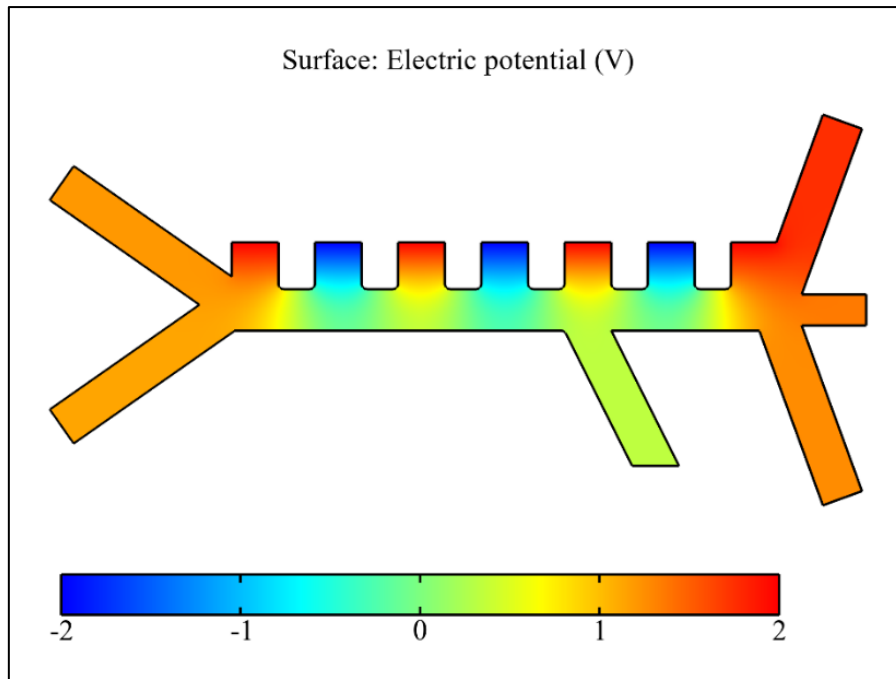


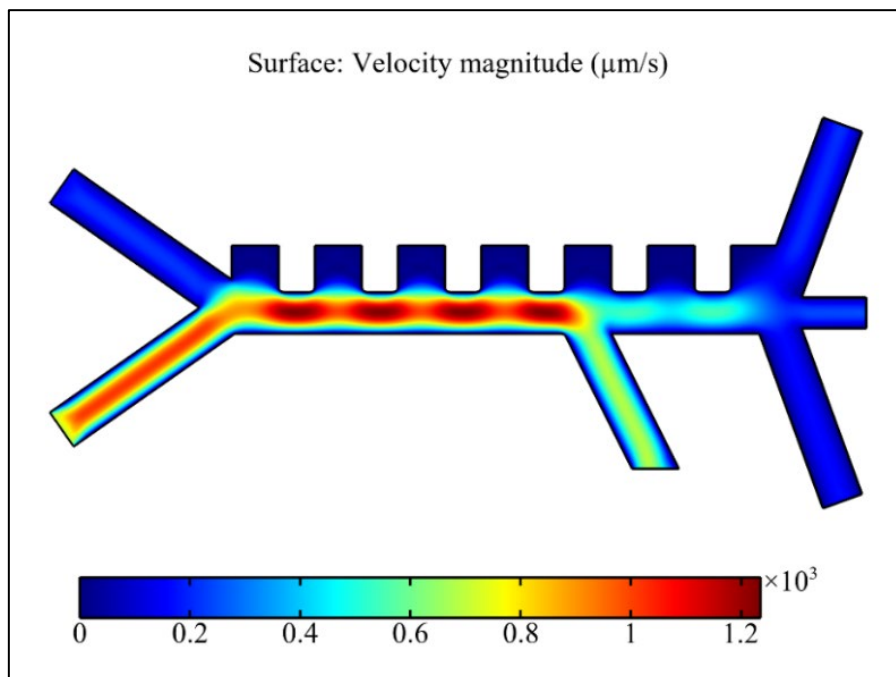
**Figure 7.11:** The two-dimensional meshed model of the dielectrophoretic separation channel which separates CTCs, RBCs and WBCs

### 7.2.2 Results from Study 1

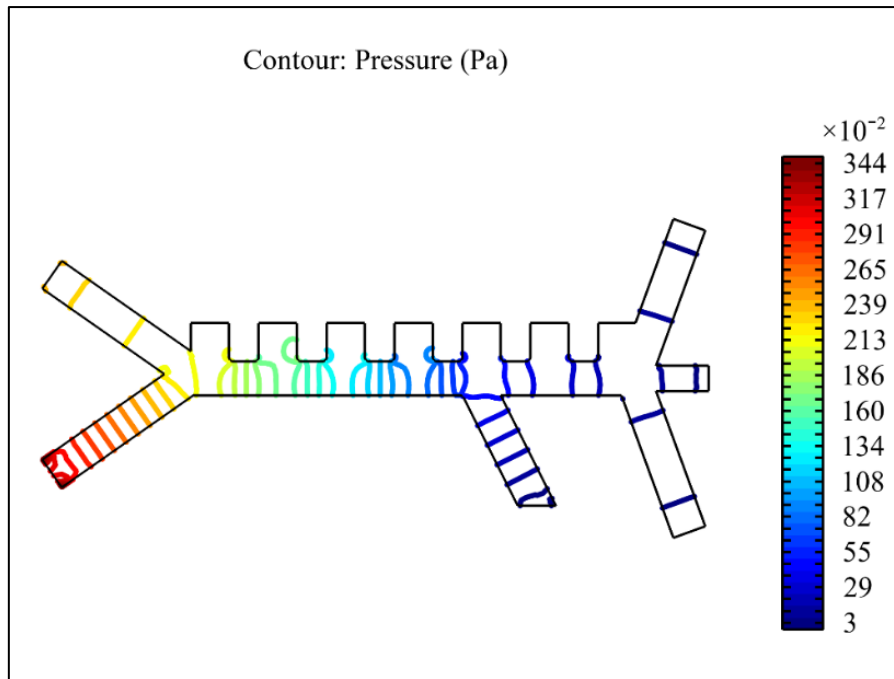
The study that solves for the velocity magnitude, pressure, and AC electric potential. The outcomes of this study for the microchannel that is intended to separate CTCs from WBCs and RBCs are shown in **Figure 7.12(a), (b) and (c)**.



(a)



(b)



(c)

**Figure 7.12:** Spatial variation of (a) surface electric potential (V), (b) velocity ( $\mu\text{m/s}$ ), and (c) pressure (Pa)

### 7.2.3 Results from Study 2

For the estimation of the particle trajectories in the flow without application of any electric field which means, no DEP force will act on the particles, so that all particles (CTCs and RBCs) follow the same path; study 2 was evaluated. The observed result is shown in **Figure 7.13**.

The CTCs, RBCs and WBCs mixture velocity at the upper inlet (inlet 1) was kept fixed at  $150\mu\text{m/s}$  and the buffer fluid (deionized water) velocity at the lower inlet (inlet 2) was kept fixed at  $700\mu\text{m/s}$ .

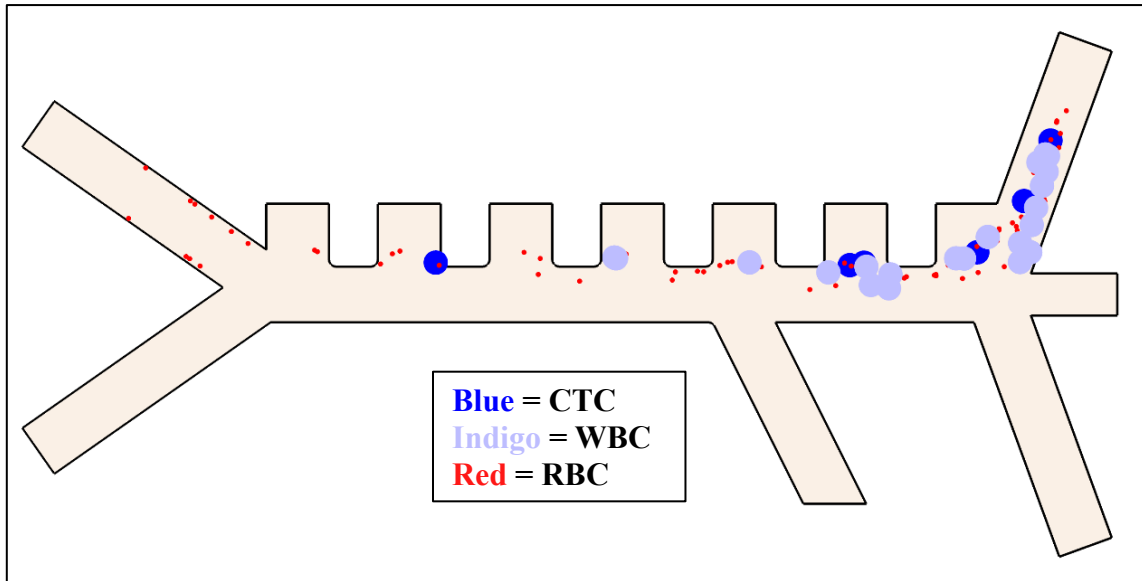


**Figure 7.13:** Particle Trajectories without application of any electric field

Here in **Figure 7.13** the blue dots represent CTC; indigo dots represent WBC and the red dots represent RBC. It can be seen that as there is no electric field applied there is no formation of DEP force as a result of which all the particles follow the same path and move out through the same outlet.

#### ***7.2.4 Results from Study 3***

Study 3 estimates the particle trajectories in the flow after application of electric field which means, DEP force will act on the particles, as a result of which different particles follow different path depending on the force, they experience which is proportional to the diameter of the particle itself. The observed result is shown in **Figure 7.14**. Here the applied electric field was 4V peak-to-peak with the CTCs, RBCs and WBCs mixture velocity at the upper inlet (inlet 1) was kept fixed at 150  $\mu\text{m/s}$  and the buffer fluid (deionized water) velocity at the lower inlet (inlet 2) was kept fixed at 700 $\mu\text{m/s}$ .

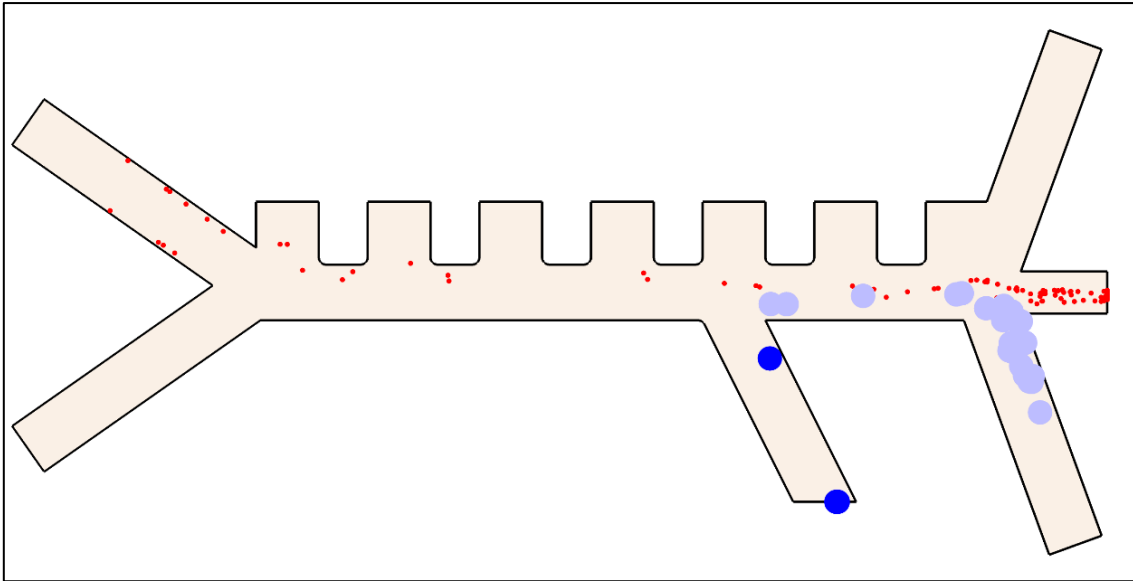


**Figure 7.14:** Particle Trajectories after application of non-uniform electric field (4V peak-to-peak)

### ***7.2.5 Analysis of the Results from Simulation of the Microfluidic Channel using ANFIS***

The following data in **Table 7.2** were obtained for the microfluidic channel that separates CTCs from WBCs and RBCs from simulations in COMSOL. Here the distribution values 0,1,2,3,4 and 5 represent no particles, only RBCs, WBCs and RBCs mixture, all three particles mixture, CTCs and WBCs mixture, only CTCs respectively at the outlet 1.



**Table 7.2** Obtained Outputs with Respect to Inputs in COMSOL

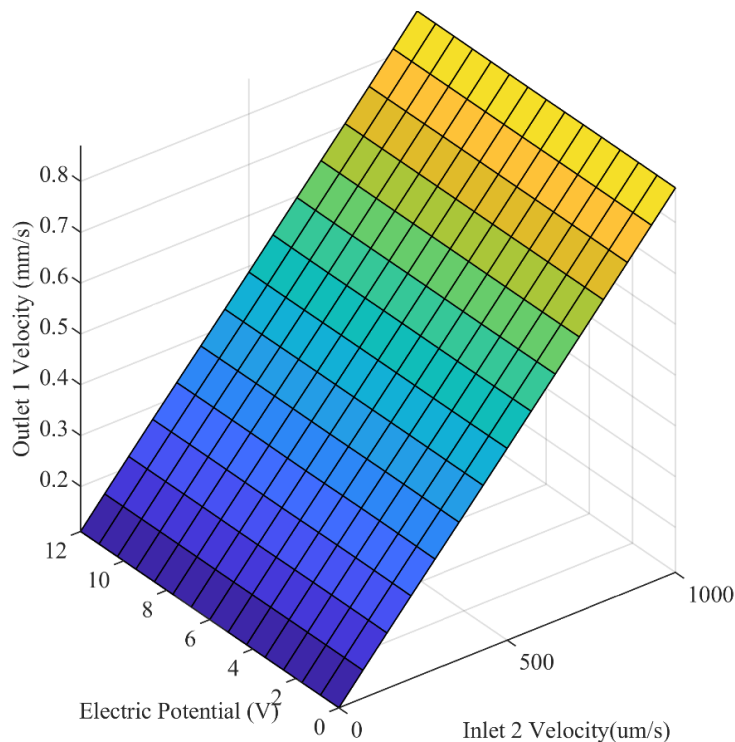
<b>Inlet 2 Velocity (<math>\mu\text{m/s}</math>)</b>	<b>Peak-to-Peak Voltage (V)</b>	<b>Distribution</b>	<b>Pressure (Pa)</b>	<b>Outlet Velocity (<math>\mu\text{m/s}</math>)</b>
0	0-12	0-3	0.67	110
50	0-12	0-3	0.8	150
100	0-12	0-3	0.92	190
150	0-12	0-3	1.05	230
200	0-12	0-3	1.26	260
250	0-12	0-3	1.48	300
300	3	4	1.71	340
300	4-12	0-3	1.71	340
350	3	5	1.93	380
350	4	4	1.93	380
350	5-12	0-3	1.93	380
400	3	5	2.15	410
400	4	4	2.15	410
400	5-12	0-3	2.15	410
450	3-4	5	2.37	450
450	5	4	2.37	0.45
450	6-12	0-3	2.37	450
500	3-4	5	2.59	490
500	5	4	2.59	490
500	6-12	0-3	2.59	490
550-600	4	5	2.82-3.04	530-560
550-600	5-6	4	2.82-3.04	530-560
650	4-5	5	3.26	600
650	6	4	3.26	600
700-850	4-5	5	3.48-4.15	640-750
700-850	6-7	4	3.48-4.15	670-750
900-1000	4-6	5	4.37-4.81	790-870
900-1000	7-8	4	4.37-4.81	790-870
900-1000	9-12	0-3	4.37-4.81	790-870

In the neuro-fuzzy toolbox of MATLAB the following data were fed:

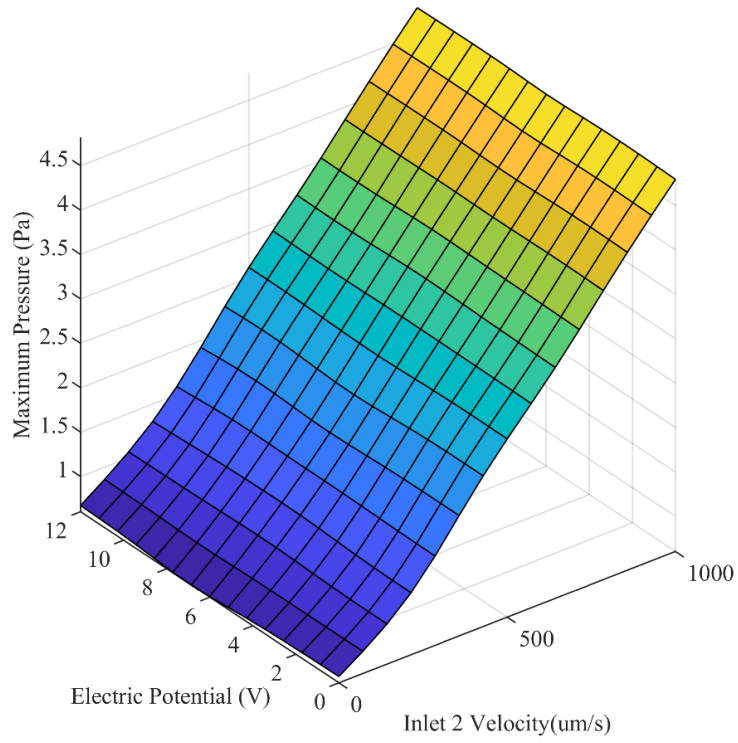
- Buffer fluid velocity at inlet 2 and electric potential given as inputs.
- Maximum pressure, outlet 1 velocity and distribution of the particles given as outputs.

Though the training process Neuro-Fuzzy Designer predicts outputs for different inputs given to the system. Increasing the number of membership functions of the input increases accuracy but sacrifices more computing power and time required for computation. 90% of the data was used for training and 10% was used for testing and RMSE was found to be 0.42. The following figures were generated as given in **Figure 7.15**.

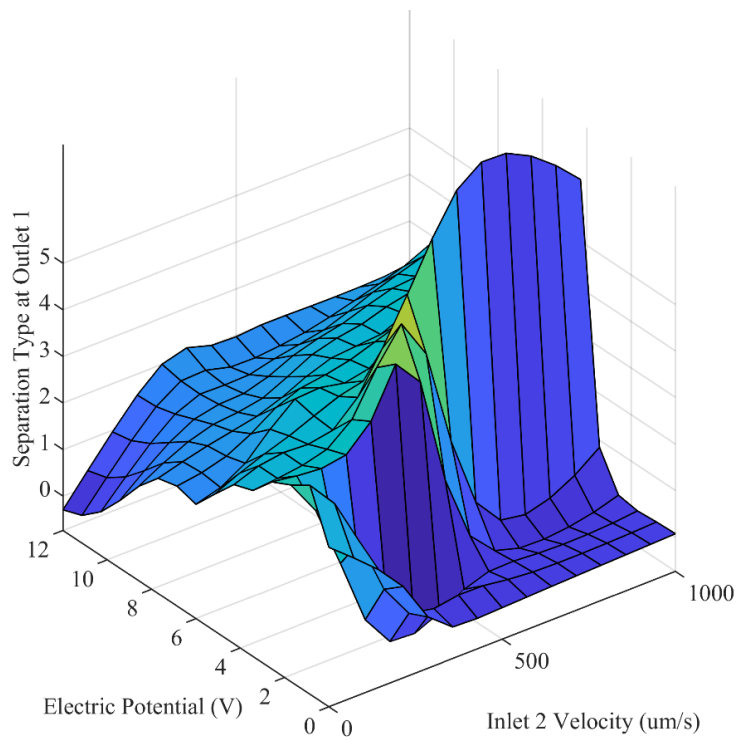
The Neuro-Fuzzy Designer resulted three 3D graphics that shows the relationship between input and output parameters with the help of neural network prediction and fuzzy logic rules. **Figure 7.15(a)** and **Figure 7.15(b)** shows the fluid velocity of the buffer fluid at inlet 2 effecting the outlet 1 velocity and maximum pressure in the microfluidic channel linearly. However, the effect of the highest electric potentials of the electrodes on the outlet 1 velocity and maximum pressure in the microfluidic chip is less. In **Figure 7.15(c)**, the effect of fluid velocity of inlet 2 over the separation profile of the CTCs is non-linear. The effect of the highest electric potentials of the electrodes on the separation profile is also non-linear.



**(a)**



(b)



(c)

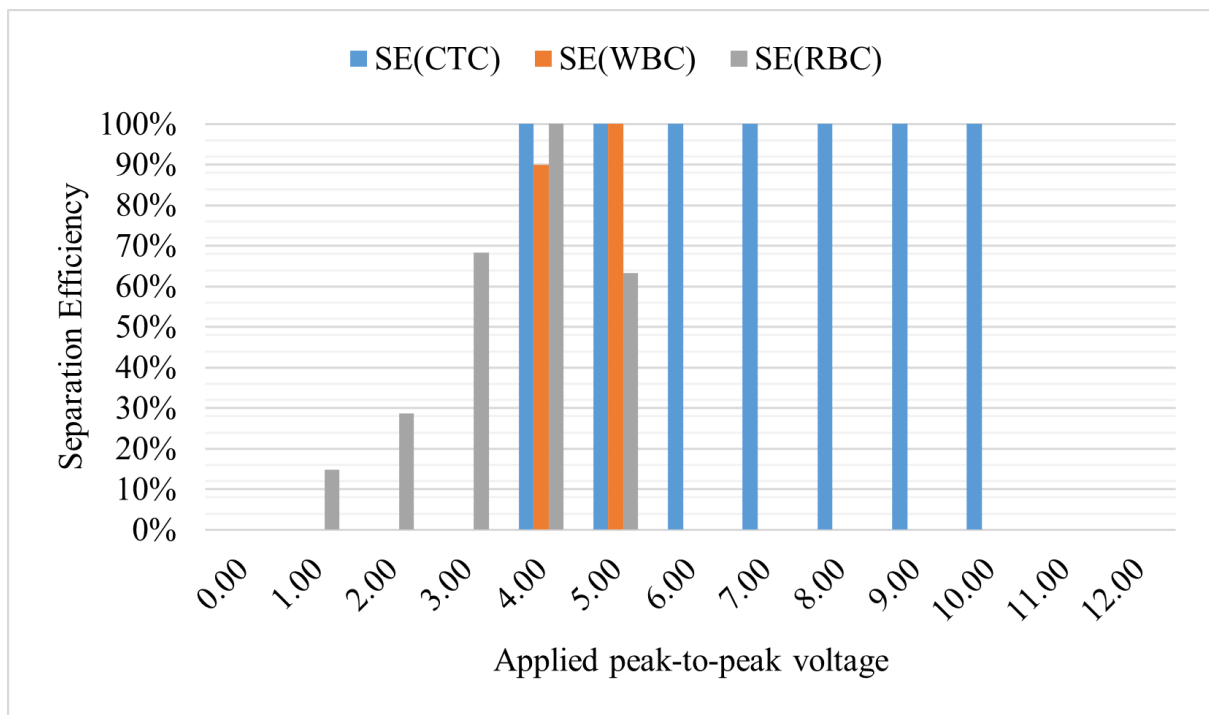
**Figure 7.15:** Effect of the buffer fluid velocity at inlet 2 and electric potential of the electrodes on (a) outlet 1 fluid velocity ( $\mu\text{m/s}$ ), (b) maximum pressure (Pa) on the microfluidic channel, and (c) separation of CTCs, RBCs and WBCs

### 7.2.6 Separation Efficiency (SE) and Separation Purity (SP) of the Microfluidic Channel

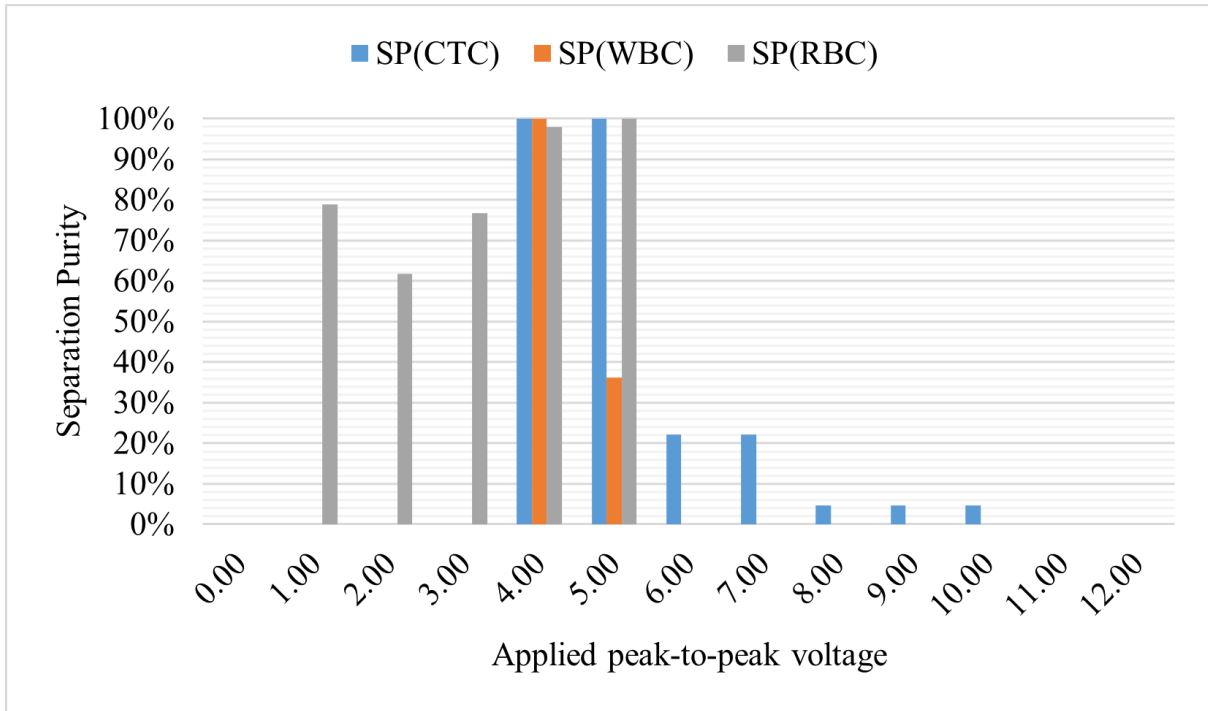
$$SE(CTC) = \frac{\text{Number of CTCs at outlet 1}}{\text{Number of CTCs at inlet 1}} \quad (7.3)$$

$$SP(CTC) = \frac{\text{Number of CTCs at outlet 1}}{\text{Number of CTCs, WBCs and RBCs at outlet 1}} \quad (7.4)$$

The total number of CTCs, RBCs and WBCs given as input into the channel were 6, 101 and 21 respectively. **Figure 7.16** depicts the performance metrics as SE and SP of the microfluidic channel with respect to applied voltage.



(a)



(b)

**Figure 7.16:** Variation of (a) SE, and (b) SP of CTCs, RBCs and WBCs with respect to applied peak-to-peak voltage electrodes (Keeping Inlet 1 velocity - 150um/s, Inlet 2 velocity - 700um/s)

# Chapter 8

## Conclusion

Microfluidic channels based on Lab-on-a-chip technology with the help of Dielectrophoresis, that can be potential tools for efficient separation of CTCs from blood cells for feasible input parameters has been proposed in this work. Microfluidics has made enormous progress in cell separation applications, utilizing its numerous inherent benefits such as increased sensitivity and spatial resolution, low sample volume, and cheap device cost. Despite the recent advent of microfluidic technology, existing microfluidic techniques for blood-based separations have a number of limitations, including time-consuming sample preparation, poor throughput, and clogging difficulties, which frequently limit separation performance. From 231 simulation results, and analyzing the ANFIS results it has been observed that for capturing CTCs from RBCs in the first microfluidic channel through outlet 3 with highest velocity of  $377\mu\text{m/s}$ , inlet 2 fluid velocity of  $1000\mu\text{m/s}$ , and 18 V peak-to-peak applied voltage on the electrodes at the first-phase separation region keeping 4V peak-to-peak applied voltage at the second phase electrodes is required. A desirable separation where all the CTCs would be separated within the first-phase separation region before going for a second-phase separation region is occurring when inlet 2 fluid velocity is  $500\mu\text{m/s}$ , applied voltage on the electrodes at the first-phase separation region and second phase are 8 V peak-to-peak and 4V peak-to-peak respectively. From 273 simulation results, and analyzing the ANFIS results it has been observed that the second microfluidic channel that separates CTCs from WBCs and RBCs inlet 2 velocity of  $1000\mu\text{m/s}$  with 12 V peak-to-peak applied voltage on the electrodes with 100 kHz AC should be provided to get the maximum separation of the CTCs from WBCs and RBCs with the highest velocity of  $870\mu\text{m/s}$  at outlet 1. However, maximum separation of CTCs can also be achievable with lower applied voltages on the electrodes which were mentioned before for both the microfluidic channels but the detection/ isolation process time will be compromised. Since the input and output relationship of a microfluidic channels were investigated in this work which suggested input parameters for attaining desirable separation of CTC particles. As a full overview of the performance of the microfluidic channels for a wide range of inputs are evaluated with the help of Artificial Intelligence technique, this would make the developing process of such microfluidic channels easier and cheaper. Thus, fabrication and production of

label-free CTC detection devices in biomedical field will be benefited. The proposed channels simply require syringe pumps to function, greatly simplifying device setup and operation. This is an important factor to consider for effective commercialization and deployment in clinical settings, ensuring technicians and clinicians are able to operate the devices with minimal training and expertise.

## **8.1 Future Works**

This work introduced two microfluidic channels based of Lab-on-a-chip technology mainly with the help of Dielectrophoresis, as well as a novel analysis technique through Artificial Intelligence. However, for the advancement of this work, the following works can be done in future:

- Incorporate other techniques like Insulator-based Dielectrophoresis (i-DEP), pinched flow fractionation, magnetophoresis, acoustophoresis in microfluidic devices.
- Developing programmable integrated Lab-on-a-chip devices.
- Better optimization of the channels.
- Changing shapes of electrodes for a better output.
- Working with different particles with different parameters.
- Gain higher throughput.

## References

- [1] N. Rahmanian, M. Bozorgmehr, M. Torabi, A. Akbari, and A. H. Zarnani, "Cell separation: Potentials and pitfalls," *Prep. Biochem. Biotechnol.*, vol. 47, no. 1, pp. 38–51, 2017, doi: 10.1080/10826068.2016.1163579.
- [2] Y. H. Ghallab and W. Badawy, *Lab-on-a-chip: Techniques, Circuits, and Biomedical Applications*. 2010.
- [3] M. Kumar, A. Kumar, S. D. George, and K. Singh, "A novel microfluidic device with tapered sidewall electrodes for efficient ternary blood cells (WBCs, RBCs and PLTs) separation," *Meas. Sci. Technol.*, vol. 32, no. 11, 2021, doi: 10.1088/1361-6501/ac0f24.
- [4] W. Waheed, A. Alazzam, B. Mathew, E. A. Nada, and A. N. Al Khateeb, "A scalable microfluidic device for switching of microparticles using dielectrophoresis," *ASME Int. Mech. Eng. Congr. Expo. Proc.*, vol. 10, pp. 1–6, 2018, doi: 10.1115/IMECE201887664.
- [5] D. G. Grier, "A revolution in optical manipulation," *Nature*, vol. 424, no. 6950, pp. 810–816, 2003, doi: 10.1038/nature01935.
- [6] K. E. McCloskey, J. J. Chalmers, and M. Zborowski, "Magnetic Cell Separation: Characterization of Magnetophoretic Mobility," *Anal. Chem.*, vol. 75, no. 24, pp. 6868–6874, 2003, doi: 10.1021/ac034315j.
- [7] A. Nilsson, F. Petersson, H. Jönsson, and T. Laurell, "Acoustic control of suspended particles in micro fluidic chips," *Lab Chip*, vol. 4, no. 2, pp. 131–135, 2004, doi: 10.1039/b313493h.
- [8] A. Ashkin, J. M. Dziedzic, J. E. Bjorkholm, and S. Chu, "Observation of a single-beam gradient force optical trap for dielectric particles," *Opt. Angular Momentum*, vol. 11, no. 5, pp. 196–198, 2016, doi: 10.1364/ol.11.000288.
- [9] R. M. J. Palmer, A. G. Ferrige, and S. \* Moncada, "Optical trapping and manipulation of single cells using infrared laser beam," *Nature*, vol. 327, no. Nitric oxide release accounts for the biological activity of endothelium-derived relaxing factor, pp. 524–526, 1987.
- [10] D. Facts, *Dielectrophoresis (BOOK)*. 2005.
- [11] Jones, T. B. (1995) *Electromechanics of Particles*, Cambridge University Press, Cambridge.
- [12] Bruus, H. (2012) *Acoustofluidics 7: The acoustic radiation force on small particles*. *Lab Chip* 12, 1014–1021.}



- [13] J. Voldman, "Electrical forces for microscale cell manipulation," *Annu. Rev. Biomed. Eng.*, vol. 8, pp. 425–454, 2006, doi: 10.1146/annurev.bioeng.8.061505.095739.
- [14] J. Wang et al., "Towards disposable lab-on-a-chip: Poly(methylmethacrylate) microchip electrophoresis device with electrochemical detection," *Electrophoresis*, vol. 23, no. 4, pp. 596–601, 2002, doi: 10.1002/1522-2683(200202)23:4<596::AID-ELPS596>3.0.CO;2-C.
- [15] J. A. Ferguson, T. C. Boles, C. P. Adams, and D. R. Walt, "A fiber-optic DNA biosensor microarray for the analysis of gene expression," *Nat. Biotechnol.*, vol. 14, no. 13, pp. 1681–1684, 1996, doi: 10.1038/nbt1296-1681.
- [16] S. Fiedler, S. G. Shirley, and T. Schnelle, "a Microsystem," vol. 70, no. 9, pp. 1909–1915, 1998.
- [17] M. C. Jo and R. Guldiken, "Active density-based separation using standing surface acoustic waves," *Sensors Actuators, A Phys.*, vol. 187, pp. 22–28, 2012, doi: 10.1016/j.sna.2012.08.020.
- [18] W. Waheed, A. Alazzam, B. Mathew, N. Christoforou, and E. Abu-Nada, "Lateral fluid flow fractionation using dielectrophoresis (LFFF-DEP) for size-independent, label-free isolation of circulating tumor cells," *J. Chromatogr. B Anal. Technol. Biomed. Life Sci.*, vol. 1087–1088, no. November 2017, pp. 133–137, 2018, doi: 10.1016/j.jchromb.2018.04.046.
- [19] H. K. Chin, C. L. Yee, I. Rodriguez, C. Yang, and K. Youcef-Toumi, "Cell motion model for moving dielectrophoresis," *Anal. Chem.*, vol. 80, no. 14, pp. 5454–5461, 2008, doi: 10.1021/ac800947e.
- [20] R. Pethig and G. H. Markx, "Applications of dielectrophoresis in biotechnology," *Trends Biotechnol.*, vol. 15, no. 10, pp. 426–432, 1997, doi: 10.1016/S0167-7799(97)01096-2.
- [21] M. P. Hughes, H. Morgan, F. J. Rixon, J. P. H. Burt, and R. Pethig, "Manipulation of herpes simplex virus type 1 by dielectrophoresis," *Biochim. Biophys. Acta - Gen. Subj.*, vol. 1425, no. 1, pp. 119–126, 1998, doi: 10.1016/S0304-4165(98)00058-0.
- [22] B. Marrow et al., "Cutting Edge Communication," vol. 489, pp. 473–489, 2003.
- [23] D. Hu, H. Liu, Y. Tian, Z. Li, and X. Cui, "Sorting Technology for Circulating Tumor Cells Based on Microfluidics," *ACS Comb. Sci.*, vol. 22, no. 12, pp. 701–711, 2020, doi: 10.1021/acscombsci.0c00157.

- [24] L. E. Cortés-Hernández, Z. Eslami-S, and C. Alix-Panabières, “Circulating tumor cell as the functional aspect of liquid biopsy to understand the metastatic cascade in solid cancer,” *Mol. Aspects Med.*, vol. 72, no. July, pp. 0–1, 2020, doi: 10.1016/j.mam.2019.07.008.
- [25] Z. Çağlayan, Y. D. Yalçın, and H. Külah, “A prominent cell manipulation technique in biomems: Dielectrophoresis,” *Micromachines*, vol. 11, no. 11, 2020, doi: 10.3390/mi11110990.
- [26] J. Zhang, K. Chen, and Z. H. Fan, *Circulating Tumor Cell Isolation and Analysis*, 1st ed., vol. 75. Elsevier Inc., 2016.
- [27] M. Al-Mahasneh, M. Aljarrah, T. Rababah, and M. Alu’datt, “Application of Hybrid Neural Fuzzy System (ANFIS) in Food Processing and Technology,” *Food Eng. Rev.*, vol. 8, no. 3, pp. 351–366, 2016, doi: 10.1007/s12393-016-9141-7.
- [28] J. S. R. Jang, “ANFIS: Adaptive-Network-Based Fuzzy Inference System,” *IEEE Trans. Syst. Man Cybern.*, vol. 23, no. 3, pp. 665–685, 1993, doi: 10.1109/21.256541.
- [29] S. Krishna, F. Alnaimat, A. Hilal-Alnaqbi, S. Khashan, and B. Mathew, “Dielectrophoretic microfluidic device for separating microparticles based on size with sub-micron resolution,” *Micromachines*, vol. 11, no. 7, pp. 1–17, 2020, doi: 10.3390/MI11070653.
- [30] Y. Zhang and X. Chen, “Dielectrophoretic microfluidic device for separation of red blood cells and platelets: a model-based study,” *J. Brazilian Soc. Mech. Sci. Eng.*, vol. 42, no. 2, 2020, doi: 10.1007/s40430-020-2169-x.
- [31] F. Alnaimat et al., “Model-Based Performance Study of Dielectrophoretic Flow Separator,” *IEEE Sensors Lett.*, vol. 3, no. 6, pp. 2016–2019, 2019, doi: 10.1109/LENS.2019.2915101.
- [32] M. Aghaamoo, A. Aghilinejad, X. Chen, and J. Xu, “On the design of deterministic dielectrophoresis for continuous separation of circulating tumor cells from peripheral blood cells,” *Electrophoresis*, vol. 40, no. 10, pp. 1486–1493, 2019, doi: 10.1002/elps.201800459.
- [33] I. Ertugrul and O. Ulkir, “Dielectrophoretic separation of platelet cells in a microfluidic channel and optimization with fuzzy logic,” *RSC Adv.*, vol. 10, no. 56, pp. 33731–33738, 2020, doi: 10.1039/d0ra06271e.
- [34] A. Al-Hmouz, J. Shen, R. Al-Hmouz, and J. Yan, “Modeling and simulation of an Adaptive Neuro-Fuzzy Inference System (ANFIS) for mobile learning,” *IEEE Trans. Learn. Technol.*, vol. 5, no. 3, pp. 226–237, 2012, doi: 10.1109/TLT.2011.36.
- [35] Herbert A. Pohl, "The Motion and Precipitation of Suspensoids in Divergent Electric Fields", *Journal of Applied Physics* 22, 869-871 (1951) [https://doi: 10.1063/1.1700065](https://doi.org/10.1063/1.1700065)

- [36] Muth, E. Ueber die Erscheinung der Perlschnurkettenbildung von Emulsionspartikelchen unter Einwirkung eines Wechselfeldes. *Kolloid-Zeitschrift* 41, 97–102 (1927). doi: 10.1007/BF01428586
- [37] SCHWAN HP. Electrical properties of tissue and cell suspensions. *Adv Biol Med Phys.* 1957;5:147-209. doi: 10.1016/b978-1-4832-3111-2.50008-0. PMID: 13520431.
- [38] Pohl HA, Hawk I. Separation of living and dead cells by dielectrophoresis. *Science.* 1966 Apr 29;152(3722):647-9. doi: 10.1126/science.152.3722.647-a. PMID: 17779503.
- [39] Joe S. Crane and Herbert A. Pohl 1968 *J. Electrochem. Soc.* 115 584
- [40] Y. W. Lu, C. Sun, Y. C. Kao, C. L. Hung, and J. Y. Juang, “Dielectrophoretic crossover frequency of single particles: Quantifying the effect of surface functional groups and electrohydrodynamic flow drag force,” *Nanomaterials*, vol. 10, no. 7, pp. 1–22, 2020, doi: 10.3390/nano10071364.
- [41] O. F. Mossotti, *Mem. Mat. Fis. Soc. Ital. Sci. Modena* 24(2), 49 (1850).
- [42] Nurdan Erdem, Yagmur Yildizhan, and Meltem Elitas, “A Numerical Approach for Dielectrophoretic Characterization and Separation of Human Hematopoietic Cells,” *Int. J. Eng. Res.*, vol. V6, no. 04, pp. 1079–1082, 2017, doi: 10.17577/ijertv6is040730.
- [43] J. Cottet, O. Fabregue, C. Berger, F. Buret, P. Renaud, and M. Frénéa-Robin, “MyDEP: A New Computational Tool for Dielectric Modeling of Particles and Cells,” *Biophys. J.*, vol. 116, no. 1, pp. 12–18, 2019, doi: 10.1016/j.bpj.2018.11.021.
- [44] Y. Zhang and X. Chen, “Blood cells separation microfluidic chip based on dielectrophoretic force,” *J. Brazilian Soc. Mech. Sci. Eng.*, vol. 42, no. 4, pp. 1–11, 2020, doi: 10.1007/s40430-020-02284-8.
- [45] C. L. Kumar, A. V. Juliet, B. Ramakrishna, S. Chakraborty, M. A. Mohammed, and K. A. Sunny, “Computational Microfluidic Channel for Separation of Escherichia coli from Blood-Cells,” *Comput. Mater. Contin.*, vol. 67, no. 2, pp. 1369–1384, 2021, doi: 10.32604/cmc.2021.015116.
- [46] Y. C. Lim; A. Z. Kouzani; W. Duan (2010). *Lab-on-a-chip: a component view.* , 16(12), 1995–2015. doi:10.1007/s00542-010-1141-6.
- [47] Mohammed, Mazher Iqbal; Haswell, Steven; Gibson, Ian (2015). *Lab-on-a-chip or Chip-in-a-lab: Challenges of Commercialization Lost in Translation.* *Procedia Technology*, 20(), 54–59. doi:10.1016/j.protcy.2015.07.010
- [48] M. Farré, L. Kantiani, and D. Barceló, *Microfluidic Devices: Biosensors.* 2012.
- [49] J. W. Hong and S. R. Quake, “Integrated nanoliter systems,” *Nat. Biotechnol.*, vol. 21, no. 10, pp. 1179–1183, 2003, doi: 10.1038/nbt871.

- [50] Weibel, Douglas B.; Kruithof, Maarten; Potenta, Scott; Sia, Samuel K.; Lee, Andrew; Whitesides, George M. (2005). Torque-Actuated Valves for Microfluidics. *Analytical Chemistry*, 77(15), 4726–4733. doi:10.1021/ac048303p
- [51] Günther, Axel; Jhunjhunwala, Manish; Thalmann, Martina; Schmidt, Martin A.; Jensen, Klavs F. (2005). Micromixing of Miscible Liquids in Segmented Gas–Liquid Flow. *Langmuir*, 21(4), 1547–1555. doi:10.1021/la0482406
- [52] Garstecki, Piotr; Fischbach, Michael A.; Whitesides, George M. (2005). Design for mixing using bubbles in branched microfluidic channels. *Applied Physics Letters*, 86(24), 244108–. doi:10.1063/1.1946902
- [53] Stone, H.A.; Stroock, A.D.; Ajdari, A. (2004). ENGINEERING FLOWS IN SMALL DEVICES. , 36(1), 381–411. doi:10.1146/annurev.fluid.36.050802.122124
- [54] Squires, Todd; Quake, Stephen (2005). Microfluidics: Fluid physics at the nanoliter scale. , 77(3), 977–1026. doi:10.1103/revmodphys.77.977
- [55] Whitesides, George M. (2006). The origins and the future of microfluidics. , 442(7101), 368–373. doi:10.1038/nature05058
- [56] Wheeler, Aaron R.; Thordset, William R.; Whelan, Rebecca J.; Leach, Andrew M.; Zare, Richard N.; Liao, Yish Hann; Farrell, Kevin; Manger, Ian D.; Daridon, Antoine (2003). Microfluidic Device for Single-Cell Analysis. *Analytical Chemistry*, 75(14), 3581–3586. doi:10.1021/ac0340758
- [57] Gale, Bruce; Jafek, Alexander; Lambert, Christopher; Goenner, Brady; Moghimifam, Hossein; Nze, Ugochukwu; Kamarapu, Suraj (2018). A Review of Current Methods in Microfluidic Device Fabrication and Future Commercialization Prospects. *Inventions*, 3(3), 60–. doi:10.3390/inventions3030060
- [58] Adelina-Gabriela Niculescu; Cristina Chircov; Alexandra Cătălina Bîrcă; Alexandru Mihai Grumezescu; (2021). Fabrication and Applications of Microfluidic Devices: A Review. *International Journal of Molecular Sciences*, (), -. doi: 10.3390 / ijms22042011
- [59] Guckenberger, David J.; de Groot, Theodorus E.; Wan, Alwin M. D.; Beebe, David J.; Young, Edmond W. K. (2015). Micromilling: a method for ultra-rapid prototyping of plastic microfluidic devices. *Lab Chip*, 15(11), 2364–2378. doi:10.1039/c5lc00234f
- [60] L. A. Zadeh, “Fuzzy logic,” *Comput. Complex. Theory, Tech. Appl.*, vol. 9781461418, pp. 1177–1200, 2013, doi: 10.1007/978-1-4614-1800-9\_73.
- [61] R. Pethig, “Dielectrophoresis: Status of the theory, technology, and applications,” *Biomicrofluidics*, vol. 4, no. 2, pp. 1–35, 2010, doi: 10.1063/1.3456626.

- [62] E. Chiriac, M. Avram, and C. Bălan, “Manipulation of particles using dielectrophoresis in a microchannel,” *Rom. J. Inf. Sci. Technol.*, vol. 24, no. 2, pp. 213–221, 2021.
- [63] Y. Guan et al., “Dielectrophoresis separation of platelets using a novel zigzag microchannel,” *Micromachines*, vol. 11, no. 10, 2020, doi: 10.3390/mi11100890.
- [64] U. Pliquet, “Joule heating during solid tissue electroporation,” *Med. Biol. Eng. Comput.*, vol. 41, no. 2, pp. 215–219, 2003, doi: 10.1007/BF02344892.